Genome-wide analysis reveals PhoP regulates pathogenicity in *Riemerella anatipestifer*

Regulation of PhoP in *Riemerella anatipestifer*

Yang Zhang[1¶], Ying Wang[1,4¶], Yanhao Zhang[1], Xiangchao Jia[1], Chenxi Li[1], Zutao Zhou[1,2,3], Sishun Hu[1,2,3], Zili Li[1,2,3*]

[1] State Key Laboratory of Agricultural Microbiology, College of Veterinary Medicine, Huazhong Agricultural University. Wuhan, Hubei, 430070, China

[2] Key Laboratory of Preventive Veterinary Medicine in Hubei Province, Wuhan, Hubei, 430070, China

[3] Key Laboratory of Development of Veterinary Diagnostic Products, Ministry of Agriculture of the People's Republic of China, Wuhan, Hubei, 430070, China

[4] College of Veterinary Medicine, Shanxi Agricultural University, Taigu, Jinzhong, 030801, China

¶ equal contribution

*lizili@mail.hzau.edu.cn (ZL)

Yang Zhang: Conceptualization, Data Curation, Formal Analysis, Investigation, Methodology, Project Administration, Resources, Software, Supervision, Validation, Visualization, Writing – Original Draft Preparation, Writing – Review & Editing

Ying Wang: Conceptualization, Data Curation, Formal Analysis, Investigation, Methodology, Project Administration, Resources, Validation, Visualization, Writing – Original Draft Preparation

Yanhao Zhang: Investigation

Xiangchao Jia: Investigation

Chenxi Li: Investigation

Zutao Zhou: Methodology, Resources

Sishun Hu: Methodology, Project Administration

Zili Li: Funding Acquisition, Methodology, Resources, Supervision, Writing – Review & Editing

Abstract

Duck infectious serositis, also known as the *Riemerella anatipestifer* disease infects domestic ducks, geese, turkeys, and wild birds. However, the regulatory mechanism of its pathogenicity remains unclear. The *phoP*/*phoR* two-component system was first reported in gram-negative bacteria in our previous research and was demonstrated to be involved in virulence and gene expression. Here, the DNA-affinity-purified sequencing (DAP-seq) was applied to further explore the regulation of *phoP*/*phoR* to pathogenicity in *R. anatipestifer*. A conserved motif was identified in the upstream of 583 candidate target genes which were directly regulated by *phoP*. To further confirm the genes which are regulated by *phoP*/*phoR*, *phoR* and *phoP,* the single-gene deletion strains were constructed. The results of transcriptome analysis using next-generation RNA sequencing showed 136 differential expression genes (DEGs) between Δ*phoP* and RA-YM, and 183 DEGs between Δ*phoR* and WT. The candidate target genes of PhoP were further identified by combining transcriptome analysis and DAP-seq. The results of DAP-seq and RNA-seq of Δ*phoP* in combination revealed that the main direct regulons of PhoP are located on the membrane and PhoP is involved in regulating aerotolerance. Using the *in vivo* duck model, the pathogenicity of Δ*phoP* or Δ*phoR* was significantly lower than that of the WT. Together, our findings provided a perception about the direct regulation of PhoP and suggested that *phoP*/*phoR* is essential for the pathogenicity of *R. anatipestifer*, and *phoP*/*phoR* is related to the aerotolerance of *R. anatipestifer*. The gene deletion strains are expected to be the candidate live vaccine strains of *R. anatipestifer* which can be used as ideal genetic engineering vector strains for the expression of foreign antigens.

Author summary

Riemerella anatipestifer is a severe pathogen in the poultry industry with high mortality in ducks and geese mainly due to acute septicemia and infectious polyserositis. A two-component system *phoP*/*phoR* was previously characterized in *R. anatipestifer*, and the *phoP*/*phoR* TCS was reported for the first time in Gram-negative bacteria. A deleted *phoP*/*phoR* in *R. anatipestifer* has been reported to almost lose its pathogenicity in ducklings. However, the mechanism of *phoP*/*phoR* regulating the virulence of *R. anatipestifer* had not been explored in detail. This study has utilized DAP-seq to explore the DNA-binding sites of PhoP as a response regulator in the global genome. Furthermore, the *phoP* and *phoR* were deleted separately and the transcriptomics of the corresponding gene-deleted strains was analyzed. A series of directly regulated genes of *phoP/phoR* TCS were determined in combination. The duckling model revealed both PhoP and PhoR as essential virulence-related factors of *R. anatipestifer*.

Introduction

The duck infectious serositis is also known as the *Riemerella anatipestifer* disease. It is one of the severe bacterial infectious diseases in the duck industry and an acute, contact, and septic infectious disease infecting domestic ducks, geese, turkeys, and a variety of poultry and wild birds [1,2]. The pathological changes of this disease are characterized by cellulosic pericarditis, perihepatic inflammation, gasbag inflammation, and meningitis. The Gram-negative bacterium, *R. anatipestifer* belongs to the family *Flavobacteriaceae* and has at least 21 serotypes [3]. The pathogenicity of *R. anatipestifer* is related to the metabolic synthesis-related genes, bicomponent system, type IX secretion system, and CRISPR-Cas system. Wang found that the biosynthesis of lipopolysaccharide (LPS) of *R. anatipestifer* is related to

the pathogenicity of the bacteria. [4]. Dou reported there was an improvement in the adhesion and invasion ability of the *R. anatipestifer* LPS gene deletion strain, but the sensitivity to duck serum complement was enhanced, and the pathogenicity of the deletion strain was more than 360 times lower than that of the wild type (WT) strain [5]. Then, *M949_RS01035* was found to be related to the biosynthesis of LPS and phenotype, virulence, and gene regulation of *R. anatipestifer* [6]. Tian *et al*. identified that DPS prevents the damage induced by H_2O_2 through iron binding, and protects *R. anatipestifer* from oxidative stress and host clearance [7]. The latest research found that *R. anatipestifer* has type IX secretion system (T9SS). The type IX secretion system proteins SprT and SprA were confirmed to be related to the pathogenicity of *R. anatipestifer*. Guo found T9SS to secrete RAYM_01812 and RAYM_04099 proteins significantly affect the pathogenicity of *R. anatipestifer*, indicating that T9SS is closely related to the virulence and secretion of the key proteins [8]. The functional components of T9SS, GldK, and GldM are reportedly related to the movement, protein secretion, and virulence of *R. anatipestifer* [9–11].

The ability of pathogens to sense and respond to the environmental change encountered within-host is generally believed to be essential for sustaining the bacterium within its pathogenicity and survivability [12]. The classic two-component system (TCS) consists of two parts: histidine kinase sensing protein, which is usually membrane-bound and acted as an environmental sensor with a signal receiver domain, and response regulatory protein that often functions as a transcription regulatory factor with a DNA-binding domain [12]. Among them, the phosphorylated histidine kinase sensing protein phosphorylates by transferring the phosphorylation group to the reaction regulatory protein in the cytoplasm. The

94 phosphorylated reaction protein causes the expression of the bacterial gene [13].

95 Discovering the gene regulation mediated by TCSs of bacterial pathogens is essential for
96 understanding the mechanisms of bacterial survival and infection. *Mycobacterium*
97 *tuberculosis* PhoP/PhoR TCS regulates ESAT-6 secretion and affects virulence [14].
98 PhoP/PhoR regulates the phosphate balance of Gram-positive bacteria such as *Bacillus*
99 *subtilis* and *Bacillus anthracis* [15,16]. PhoP/PhoQ TCS regulates the transcription of
100 virulence genes in Gram-negative pathogens, such as *E. coli*, *Shigella*, *Yersinia pestis,* and
101 *Salmonella typhimurium* [17–19]. The two-component systems ArsR and Sthk are virulence-
102 related genes of *R. anatipestifer* [20]. *RAYM_RS09735*/*RAYM_RS09740* (*phoR*/*phoP*) double
103 gene deletion strain which was constructed in our previous research. It is the first PhoP/PhoR
104 TCS reported in Gram-negative bacteria [21]. The results of animal experiments showed that
105 the double gene deletion strain completely lost its pathogenicity to ducklings, so TCS can be
106 speculated to be involved in the virulence of *R. anatipestifer*. Analysis of RNA-seq indicated
107 that *RAYM_RS09735*/*RAYM_RS09740* was the PhoP/PhoR two-component system, and the
108 results of differential expression gene analysis showed that the TCS was a global regulatory
109 factor of *R. anatipestifer*. This is the first report that PhoP/PhoR in Gram-negative bacteria,
110 and is essential for the virulence of *R. anatipestifer*.
111 The characteristics of the direct regulatory ability of the RR's DNA-binding are generally
112 studied to further study the regulatory mechanism of TCS in pathogenic bacteria. Hence, the
113 ChIP assay is routinely used for investigating the binding sites of RR in the global genome *in*
114 *vivo* [22–25]. However, there are some defects in this method, one being that the ChIP-level
115 antibody against RR is not easily available. Due to the unknown nature of the signals sensed

by the majority of TCS, it is difficult to simulate the phosphorylation regulation *in vivo* to explore the phosphorylation regulation mechanism. Generally, HK is phosphorylated via transferring the phosphorylation group to the effector response regulator after receiving external signals, and the phosphorylated RR begins to regulate the target genes. Therefore, in this study, DNA-affinity-purified sequencing was applied to explore the direct regulation mechanism of PhoP *in vitro* [26,27]. This assay allows us to mimic the RR phosphorylation via activation by small-molecule donors like acetyl-phosphate to find the genes affected directly by the regulators.

In this study, the *phoP* and *phoR* single-gene deletion strains were further constructed based on the construction of the *phoP*/*phoR* double gene deletion strain, and the mechanism of regulating the virulence of *R. anatipestifer* was studied by combining DAP-seq and RNA-seq. On the one hand, our data laid a foundation for clarifying the role of the *phoP*/*phoR* two-component system in the pathogenic process of *R. anatipestifer*, providing a new sight into the regulation of PhoP to aerotolerance in *R. anatipestifer*, and provided a theoretical basis for discovering new drug targets. This direct and global exploration of the mechanism of *phoP* provided a model for gene regulation in *R. anatipestifer* and other pathogens and might explain how these response regulators cross-talk in other pathogens. Establishing a model for transcriptional regulation can provide a technical platform for the study of mining new virulence factors, diagnostic markers, and vaccine candidate antigens.

Results

Genome-wide identification of PhoP binding sites in *R. anatipestifer* by DAP-seq

The PhoP/PhoR TCS has been characterized by next-generation RNA sequencing in our previous study. It indicated that almost 1/3 of genes in *R. anatipestifer* are under the regulation of PhoP/PhoR at the transcriptional level [21]. While a few genes were chosen for testing the PhoP binding of their promoters before, the biophysical interactions between PhoP and the promoter regions of the genes controlled remain unclear. Furthermore, due to the limitation of lacking an antibody against PhoP in *R. anatipestifer*, a self-made rabbit antibody was used against PhoP to proceed with Chromatin Immunoprecipitation sequencing (ChIP-seq). However, the result was barely satisfactory suggesting that the purity and sensitivity of the self-made antibody are unable to achieve the level of ChIP. Due to these limitations, the DNA-affinity-purified sequencing (DAP-seq) was utilized for investigating the PhoP-binding region on the whole genome of *R. anatipestifer* which could effectively avoid the disadvantage of lacking antibodies and indirect PhoP binding *in vivo*.

The DAP-seq analysis of His_6-PhoP identified 583 enriched peaks covering the upstream regions of 764 genes. These peaks were randomly distributed along the *R. anatipestifer* genome as shown in Figure 1. The MEME suite tools were used for probing for the overrepresented sequences near the center of 583 screened peaks, and a conserved motif was generated around 579 peaks (Fig 2B). Remarkably, compared to the prokaryote motifs database, the motif enriched from PhoP is highly similar to the motif of ArcA from the *E. coli* K-12 (Fig 2A), which regulates a wide variety of aerobic enzymes under anaerobic conditions [25,28–30]. The ability to survive oxidative stress might contribute to the virulence of

159 pathogens, especially for the anaerobic bacteria, because the bacteria must be capable of
160 surviving the oxidative stress from the host defenses, particularly in the relatively aerobic
161 tissue of the air sacs during an infection [31,32].

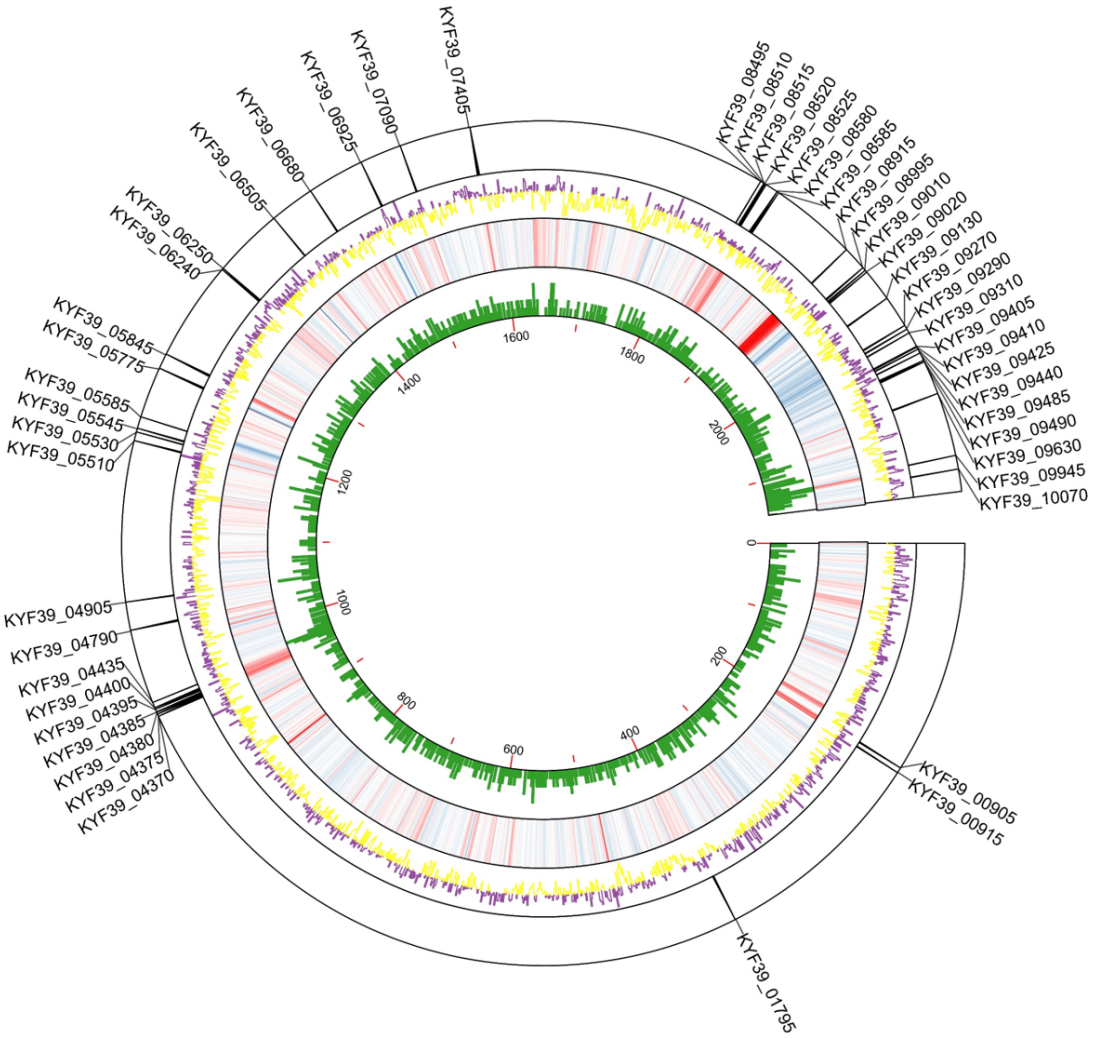

162

163 **Figure 1. Genome-wide overview of the data generated by DAP-seq and RNA-seq.** The
164 DAP-seq analysis reveals the enrichment of PhoP binding sites throughout the *Riemerella*
165 *anatipestifer* RA-YM genome. The purple and yellow line track represents the read coverage
166 of PhoP-bound sequences throughout the *R. anatipestifer* RA-YM chromosome, shown as
167 count per million reads. The regions of the PhoP-binding DNA produced 583 peaks covering
168 the upstream regions of 764 genes. The heatmap track represents the RNA-seq data by $\log_2$

fold change of the expression when Δ*phoP* was compared to RA-YM. The green track showed the gene density in RA-YM. The outmost layer of the circle shows the PhoP direct regulons. The graph was visualized by TBtools [33].

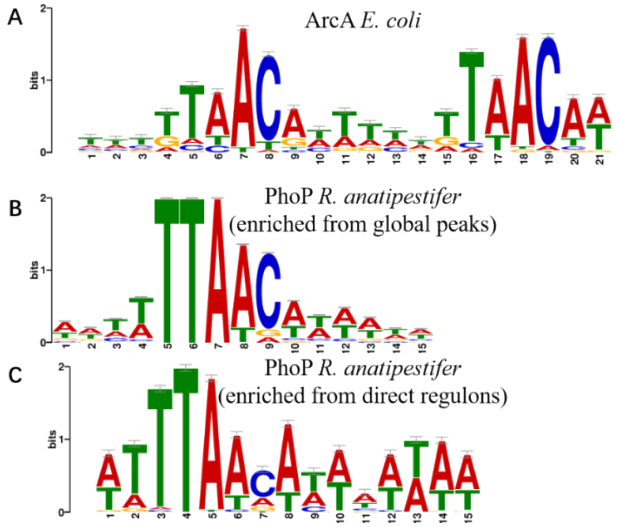

Figure 2. The most enriched motifs for the PhoP DAP-seq dataset. (A) The DNA-binding motif of ArcA in *Escherichia coli str. K-12 substr. MG1655*. (B) DNA binding motif enriched from 583 peaks that cover the upstream regions of 764 genes in RA-YM. (C) DNA binding motif enriched from the peaks covering the upstream regions of 50 candidate PhoP-binding genes that are differentially expressed in Δ*phoP*. The most conserved nucleotides are TTTAACA. The motifs were generated using MEME (https://meme-suite.org/meme/).

To validate the credibility of the DAP-seq data, the binding locus upstream of the PhoP/PhoR operon was first validated by the electrophoretic mobility shift assay (EMSA). For the majority of two-component systems, a self-regulation mechanism exists [34], and the DAP-seq data was found to generate a distinct peak upstream of *phoP*/*phoR*. Consistent with the DAP-seq and motif predicted, the EMSA assay demonstrated PhoP to bind a 35-nt region in

the region from -156 to -121 upstream of *phoP*/*phoR* (Fig 3). In addition, we sought to investigate whether the DNA-binding domain of PhoP could bind the target DNA alone *in vitro*. However, the EMSA results indicated that only the DNA-binding domain (DBD) of PhoP is not involved in the DNA binding function (Fig 3B). Subsequently, the band shifts were observed with the promoter regions of four annotated candidate genes (*moxR*, *KYF39_06865*, *dnaG,* and *dedA*) as shown in Figure 4. In other research about TCS, phosphorylation has been reported to stimulate the DNA binding ability of RR, but previous reports have also shown phosphorylation to not affect the DNA binding activity *in vitro* [35]. Therefore, the phosphorylation-treat group was added to the EMSA when validating the binding regions upstream of *moxR* and *dnaG* (Fig 4A and 4B)., The results indicated that the PhoP-binding ability of *R. anatipestifer in vitro* was not phosphorylation-dependent while the phosphorylation of *phoP* was confirmed by Phos-tag SDS-PAGE as shown in Figure S2 [36].

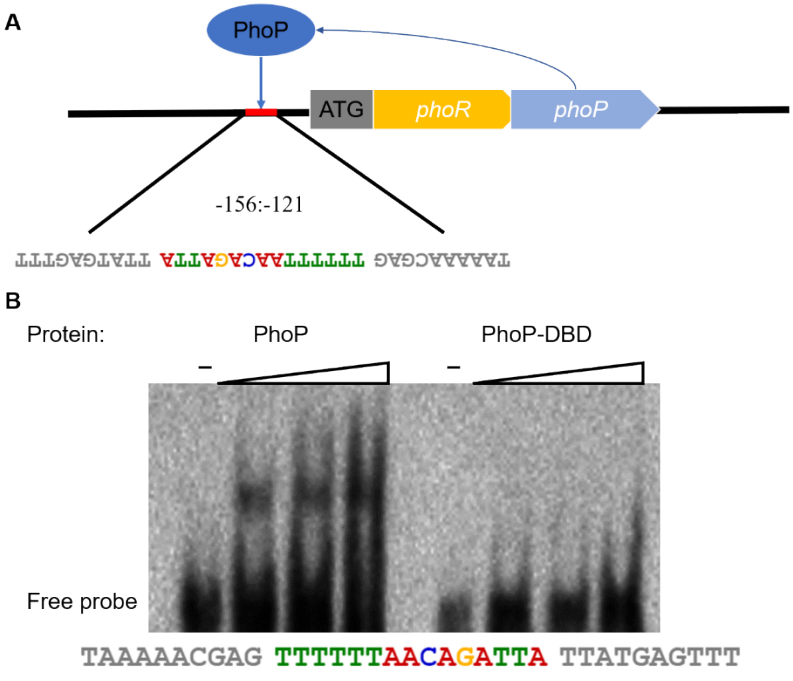

198 **Figure 3. Determination of PhoP self-regulation.** (A) The PhoP binds the upstream regions
199 of its operon to self-regulate. (B) The purified PhoP and PhoP-DBD were used for EMSAs
200 with the target DNA from the promoter region of the PhoP/R TCS. The predicted PhoP
201 binding site is noted below EMSA, and the conserved motif is highlighted in color.

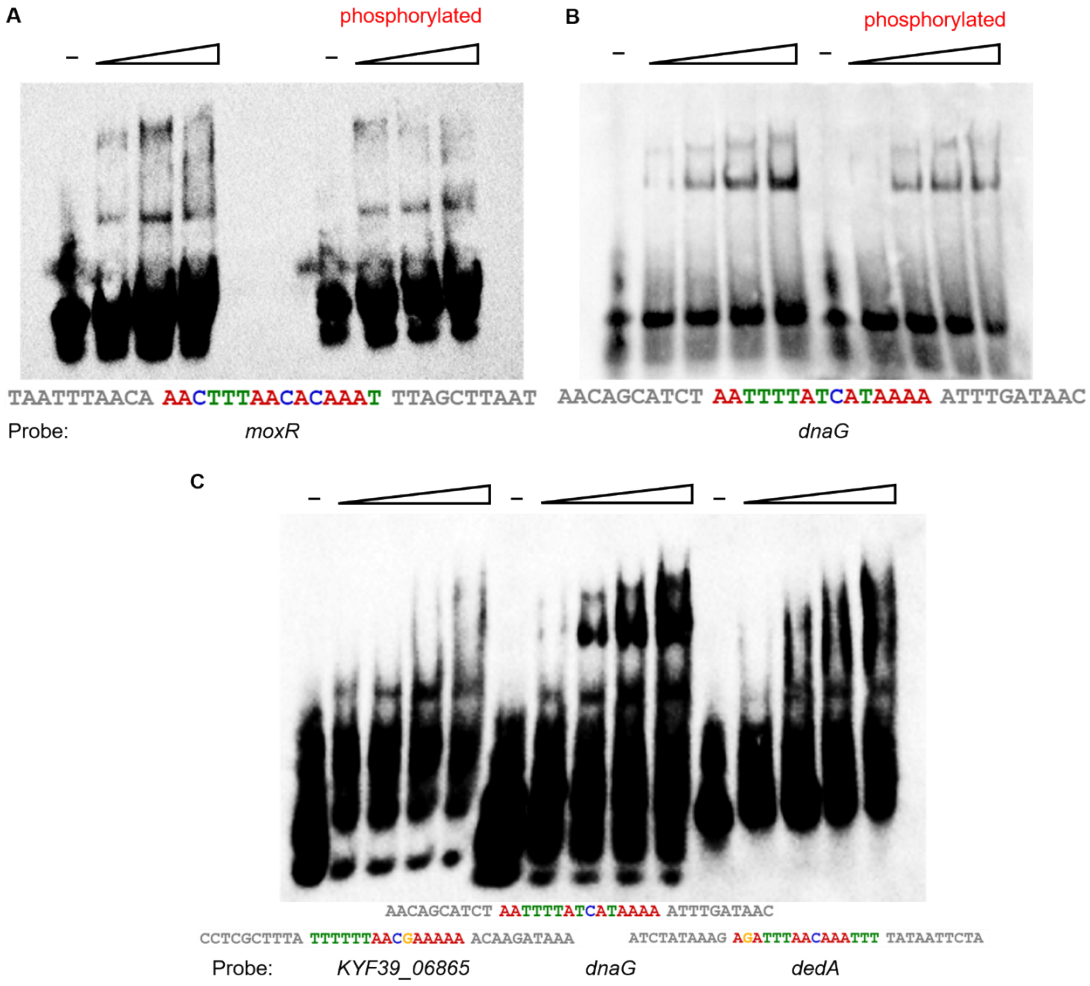

202

203 **Figure 4. Identification of PhoP binding to the upstream regions of selected genes via**
204 **EMSA.** (A and B) Purified PhoP (phosphorylated by acetyl phosphate or not) was used for
205 EMSAs with the target DNA from the promoter regions of *moxR* and *dnaG*. The predicted
206 PhoP binding site is noted below EMSA, and the conserved motifs are highlighted in color
207 respectively. (C) Purified PhoP was used for EMSAs with the target DNA from the promoter

208 regions of *KYF39_06865* (*TonB-dependent receptor*), *dnaG,* and *dedA*. The predicted PhoP
209 binding sites are noted below EMSA, and conserved motifs are highlighted in color.

210 Transcriptome characterization of PhoR and PhoP in *R. anatipestifer*

211 Our previous research has constructed a *phoP*/*phoR* double-gene deleted strain, and analyzed
212 its related phenotypic characteristics and transcriptome [21]. However, due to the
213 incompleteness of the reference genome in the previous version, the reference genome of RA-
214 YM was updated with PacBio sequencing as a reference genome (GenBank: CP079205.1)
215 and the transcriptome data of the Δ*phoP*/*phoR* double-gene deletion strain was re-processed.
216 Subsequently, to further demonstrate the regulation mechanism of *phoP*/*phoR* in the *R.*
217 *anatipestifer*, the single-gene deleted strains of *phoR* and *phoP* were constructed via
218 homologous recombination (Fig 5), and an integrated characterization of their regulons was
219 further performed via RNA-seq. A total of 183 differentially expressed genes (DEGs) were
220 identified by Δ*phoP* strain than the WT, including 123 downregulated genes and 60
221 upregulated genes (Fig 1, 6A, and 6C). The expression of 136 genes in the Δ*phoR* strain was
222 altered compared to the WT, 45 of which were significantly downregulated and 91 were
223 significantly upregulated (Fig 6B and 6C). Independent validation of the RNA-seq data for a
224 subset of genes obtained using quantitative reverse transcription PCR (RT-qPCR), confirmed
225 the confident correlation between the high-throughput results and targeted quantification. A
226 comparison of the genes regulated by PhoR and PhoP indicated 59 genes to be differentially
227 expressed in both the mutant strains, as listed in S3 Table. Further analysis of these 59 genes
228 showed that the expression of 57 genes changed in the same pattern including 35 genes
229 downregulated and 22 genes upregulated (Fig 6D), and only two genes displayed inconsistent

regulation by PhoP and PhoR. One of the two genes is the *phoP* itself, and the other is *KYF39_06325* which is annotated as a hypothetical protein (S3 Table).

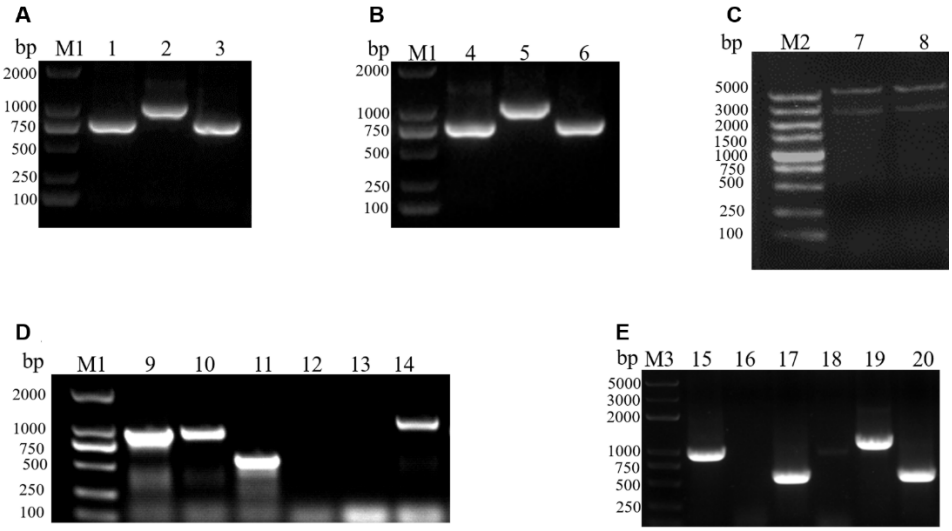

Figure 5. Construction of Δ*phoP* and Δ*phoR* mutant strains. (A) Homologous arm amplification for the *phoP* gene deletion. Lane 1: the left arm of *phoP*; Lane 2: spectinomycin resistance cassette; Lane 3: the right arm of *phoP*. (B) Homologous arm amplification for *phoR* gene deletion. Lane 4: the left arm of *phoR*; Lane 5: spectinomycin resistance cassette; Lane 6: the right arm of *phoR*. (C) Identification of the recombinant suicide plasmids for *phoP* and *phoR* gene deletion. Lane 7: *Kpn* Ⅰ and *Sac* Ⅰ digestion identification of the recombinant suicide plasmid for *phoP* gene deletion; Lane 8: *Kpn* Ⅰ and *Sac* Ⅰ digestion identification of recombinant suicide plasmid for *phoR* gene deletion. (D) *phoP* gene deletion strain identification by PCR amplification. 9. PCR product of *phoR* gene in RA-YM; 10. PCR product of *phoR* gene in Δ*phoP*; 11. PCR product of *phoP* gene in RA-YM; 12. PCR product of *phoP* in Δ*phoP*; 13. PCR product of Spec cassette in RA-YM; 14. PCR product of Spec cassette in Δ*phoP*. (E) Identification of *phoR* gene deleted strain by PCR amplification. 15. PCR product of *phoR* gene in RA-YM; 16. PCR product of Spec cassette in RA-YM; 17.

246 PCR product of *phoP* gene in RA-YM; 18. PCR product of *phoR* in Δ*phoR*; 19. PCR product

247 of Spec cassette in Δ*phoR*; 20. PCR product of *phoP* gene in Δ*phoR*; M1: DL2000 DNA

248 Marker; M2 and M3: DL5000 DNA Marker.

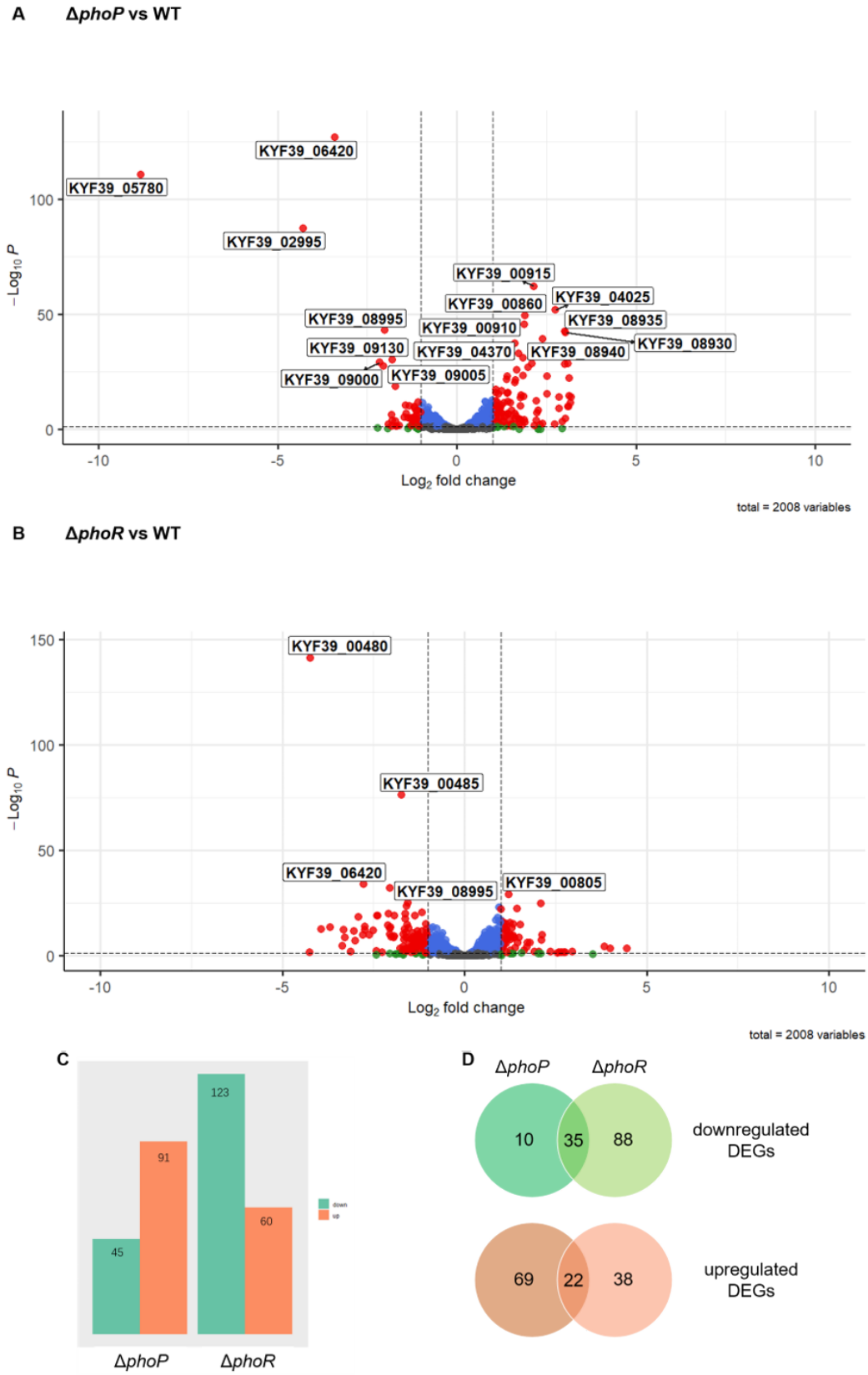

249

Figure 6. Differential expression genes of the Δ*phoR* and Δ*phoP* mutant strains compared to the WT. (A and B) Volcano plot showing differential expression of genes (DEGs) in the Δ*phoR* and Δ*phoP* respectively. Different expression genes (abs [log_2 FC > 1], false discovery rate [FDR] < 0.05) are highlighted (red). (C) Bar chart showing the number of genes whose normalized usage was significantly (Padj<0.01) reduced (cyan) or enhanced (coral) over twofold in Δ*phoP* and Δ*phoR* respectively. (D) Venn diagram showing the overlapping genes that downregulated (green system) and upregulated (orange system) in Δ*phoP* and Δ*phoR*, respectively.

Integration of transcriptome profiling with PhoP binding sites

Further, the candidate target genes that are directly regulated by PhoP were identified by combining data from the DAP-seq of PhoP and RNA-seq of Δ*phoP* (Fig 7). The differential expression of 764 genes from DAP-seq was analyzed. Surprisingly, only 50 candidate target genes were differentially expressed by the Δ*phoP* strain than the WT, including 34 upregulated genes and 16 downregulated as listed in Tables 1 and 2.

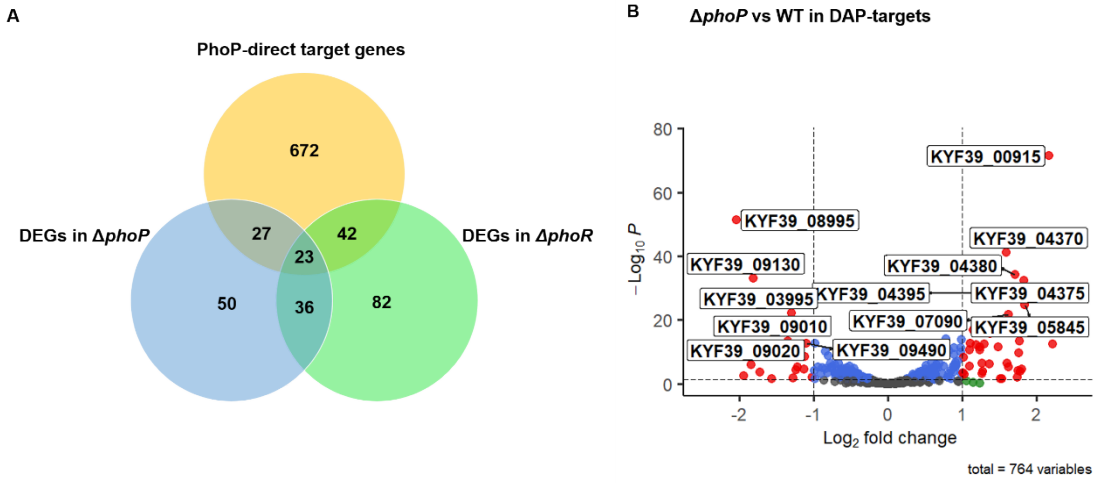

Figure 7. Combination analysis of DAP-seq and RNA-seq. (A)Venn diagram showing the overlapping genes between the DAP-seq and RNA-seq data. The PhoP-direct target genes from DAP-seq are colored in red; DEGs in Δ*phoR* and Δ*phoP* from RNA-seq are colored in green and blue respectively. (B) Volcano plot showing the differential expression of the 764 genes of the PhoP-targets. Different expression genes (abs [$\log_2$ FC > 1], false discovery rate [FDR] < 0.05) are highlighted in red.

Table 1. 34 directly downregulated/repressed DEGs by PhoP

Gene	Log2FoldChange	P-value	Annotation
KYF39_00905	3.12	1.39E-15	ABC transporter ATP-binding protein
KYF39_00915	2.14	2.00E-89	IS1595-like element ISRan1 family
KYF39_01795	1.65	6.17E-04	hypothetical protein
KYF39_04355	1.53	9.70E-03	tRNA-Glu
KYF39_04370	1.61	5.32E-32	N-acetylmuramoyl-L-alanine amidase
KYF39_04375	1.84	1.27E-18	LPS-assembly protein LptD
KYF39_04380	1.72	2.97E-37	RidA family protein
KYF39_04385	1.48	3.26E-12	hypothetical protein
KYF39_04395	1.67	2.29E-28	citrate synthase
KYF39_04400	1.16	8.51E-12	AhpC/TSA family protein
KYF39_04435	1.01	3.72E-07	type B 50S ribosomal protein L36
KYF39_04790	1.25	2.90E-07	Do family serine endopeptidase
KYF39_04905	1.50	1.47E-02	hypothetical protein
KYF39_05510	1.78	1.12E-08	adenosine deaminase
KYF39_05530	1.11	2.81E-16	hypothetical protein
KYF39_05545	1.01	2.53E-05	IS982-like element ISRa1 family transposase
KYF39_05775	1.09	1.18E-08	HAMP domain-containing histidine kinase
KYF39_05845	1.84	5.22E-04	ABC transporter ATP-binding protein/permease
KYF39_06240	1.29	3.06E-05	hypothetical protein
KYF39_06250	1.77	1.46E-11	hypothetical protein
KYF39_06505	1.25	4.09E-11	hypothetical protein
KYF39_06680	1.39	1.13E-18	GLPGLI family protein
KYF39_06925	1.38	2.58E-12	DUF4407 domain-containing protein
KYF39_07090	1.63	4.55E-30	GLPGLI family protein
KYF39_07405	2.22	4.55E-10	outer membrane beta-barrel protein
KYF39_08495	1.88	9.91E-07	nitrous oxide reductase accessory protein NosL
KYF39_08510	1.32	9.53E-05	cytochrome c
KYF39_08515	1.76	1.44E-07	c-type cytochrome
KYF39_08520	1.79	3.09E-04	hypothetical protein
KYF39_08525	1.74	3.60E-04	hypothetical protein
KYF39_08580	2.85	1.27E-02	TonB-dependent receptor
KYF39_08585	1.10	1.04E-06	alpha/beta hydrolase

KYF39_08915	3.12	3.27E-03	hypothetical protein
KYF39_09630	1.21	4.55E-07	electron transfer flavoprotein subunit alpha/FixB family protein

Table 2. 16 directly upregulated DEGs by PhoP

Gene	Log_2FoldChange	P-value	Annotation
KYF39_05585	-1.02	2.19E-03	hypothetical protein
KYF39_08995	-2.03	4.22E-35	AAA family ATPase (MoxR)
KYF39_09010	-1.33	4.32E-08	VWA domain-containing protein (BatA)
KYF39_09020	-1.44	6.99E-12	tetratricopeptide repeat protein (BatC)
KYF39_09130	-1.81	6.38E-34	GLPGLI family protein
KYF39_09270	-1.83	6.41E-08	GLPGLI family protein
KYF39_09290	-1.92	3.67E-07	hypothetical protein
KYF39_09310	-1.22	2.57E-06	HXXEE domain-containing protein
KYF39_09405	-1.12	1.24E-10	hypothetical protein
KYF39_09410	-1.72	4.30E-04	hypothetical protein
KYF39_09425	-1.29	1.07E-05	hypothetical protein
KYF39_09440	-1.13	1.90E-04	GLPGLI family protein
KYF39_09485	-1.19	2.97E-12	DNA primase (DnaG)
KYF39_09490	-1.10	1.46E-19	VTT domain-containing
KYF39_09945	-1.27	9.18E-03	hypothetical protein
KYF39_10070	-1.07	6.08E-03	hypothetical protein

PhoP directly downregulated/repressed 34 genes

Table 1 lists the 34 directly upregulated regulons in Δ*phoP* strain compared to WT, including 10 hypothetical proteins, 1 TonB-dependent receptor (TPDR) (*KYF39_08580*), 2 GLPGLI family proteins (*KYF39_06680*, *KYF39_07090*), 2 transposases (*KYF39_00915*, *KYF39_05545*), etc. Among the 30 direct upregulated genes with annotation, the most encoded proteins located in the membrane compromised TBDR, ABC transporters (*KYF39_08915*, *KYF39_05845*), βb-OMP (*KYF39_07405*), LptD (*KYF39_04375*), NosL (*KYF39_08495*), two c-type cytochromes (*KYF39_08515*, *KYF39_08510*), an N-acetylmuramoyl-L-alanine amidase (*KYF39_04370*), a FixB family protein (*KYF39_09630*),

LptD (*KYF39_04375*) and serine peptidase (*KYF39_04790*). The membrane proteins in bacteria are related to their pathogenicity and immunogenicity, like the LPS-assembly protein LptD is responsible for assembling LPS in the OM, which is an essential virulence factor in the Gram-negative bacteria [37], and can be used as the candidate of either exclusive peptide vaccines or multi-component vaccines in *Brucella melitensis* [38]. Additionally, there are two transposases in 34 directly upregulated regulons significantly, which might be due to the repression of transposase as a way for the cell to increase genome stability [39,40].

PhoP directly upregulated 16 genes

Table 2 lists the 16 directly downregulated regulons in the Δ*phoP* strain compared to the WT, including 7 hypothetical proteins, DnaG (*KYF39_09485*), 3 GLPGLI family proteins (*KYF39_09270*, *KYF39_09130*, *KYF39_09440*), and three genes (*KYF39_08995*, *KYF39_09010*, *KYF39_09020*) with locus in a complete Bacteroides aerotolerance (Bat) operon involved in pathogenicity and aerotolerance. Most notably, ArcA in *E. coli* is involved in regulation under anaerobic conditions, generating a motif similar to the motif enriched from the DAP-seq data of PhoP in *R. anatipestifer* [28]. Based on the similarity between the motif and regulatory function, *R. anatipestifer* was hypothesized to possibly adapt to the redox pressure under aerobic conditions via PhoP-regulation of the Bat operon. *Bacteroides fragilis* must enhance the survival in aerobic sites and promote opportunistic infections that induce aerotolerance and resistance to oxidative stress as physiological adaptations of *B. fragilis* to its environment [41].

In addition, we sought to identify whether a distinctive motif from the peaks in the upstream region of 50 direct regulons is different from the one enriched from the global DAP-seq data. After administering the same treatment as before, the motif generated from peaks of 50 direct regulons is approximately the same as that of 583 genes (Fig 2C), but there might be differences in the significance of the motif due to the decrease in the sample number. Subsequently, the transcriptome of Δ*phoR* was also analyzed and the Bat operon was noticed to be significantly downregulated in the absence of *phoR*. Moreover, only 4/16 of candidate genes that were directly downregulated in Δ*phoP* were not shown when only *phoR* was deleted, but the number of candidate genes that were directly upregulated in Δ*phoP* was found to be greatly reduced in Δ*phoR*. The results suggested a certain degree of inconsistency between the regulation of *phoP* and *phoR* to the downstream regulons, which might be due to the crosstalk of the phosphorylation signal transduction in *R. anatipestifer* [42]. Combined with the aforementioned data, *phoP*/*phoR* TCS can be concluded to mainly regulate the expression of the membrane proteins via PhoP-binding to the upstream regions, and regulate the aerotolerance to some extent.

Contribution of PhoR and PhoP to pathogenicity in a duck model

Since there were differences between the DEGs from the RNA-seq of Δ*phoR* and Δ*phoP* single-gene deletion strains and the previously constructed Δ*phoP*/*phoR* double gene deletion strain, we wondered whether the Δ*phoR* and Δ*phoP* strains share a similar phenotype of pathogenicity in a duck model with Δ*phoP*/*phoR* strain. Briefly, 7-day-old ducks were infected with gradient doses of Δ*phoR* and Δ*phoP* strains via fin injection, and the median

329 lethal dose (LD_{50}) was assessed. The ducks injected with the WT strain began to die on the
330 first day and the number of deaths continued to increase over the next five days. The
331 surviving ducks returned to a normal diet after 7 days of retarded behavior. The ducks
332 infected with the Δ*phoR* strain displayed favorable mental conditions, normal diet, and
333 behavior without any adverse effects. The ducks infected with the Δ*phoP* strain showed a
334 sluggish mental state after injection, preferring huddling together than moving, and gradually
335 returned to normal diet and behavior after the 4^{th} day. According to the modified Kirschner
336 method [43], the median lethal dose of WT and deletion strains were calculated. The results
337 were shown in S4 Table, the LD_{50} of RA-YM, Δ*phoP* and Δ*phoR* were 3.98×10^4 CFU/mL,
338 4.22×10^9 CFU/mL, and 1.88×10^9 CFU/mL respectively. The virulence of the Δ*phoP* strain
339 was 4.7×10^4 times lower than that of the RA-YM while the Δ*phoR* strain was 1.0×10^5
340 times lower. The results indicated that *phoP* and *phoR* were the essential virulence-related
341 genes of *R. anatipestifer*.
342 To assess the impact of *phoR* and *phoP* on the *R. anatipestifer* burden during infection, blood
343 and tissues were isolated at 24 and 48 h after infection, homogenized, and then plated to
344 enumerate CFU. There were significantly fewer bacteria both observed in the blood and
345 tissues of ducks infected with Δ*phoP* or Δ*phoR* strain respectively (Fig 9), implicating that
346 *phoR* and *phoP* were essential in the virulence of *R. anatipestifer*.

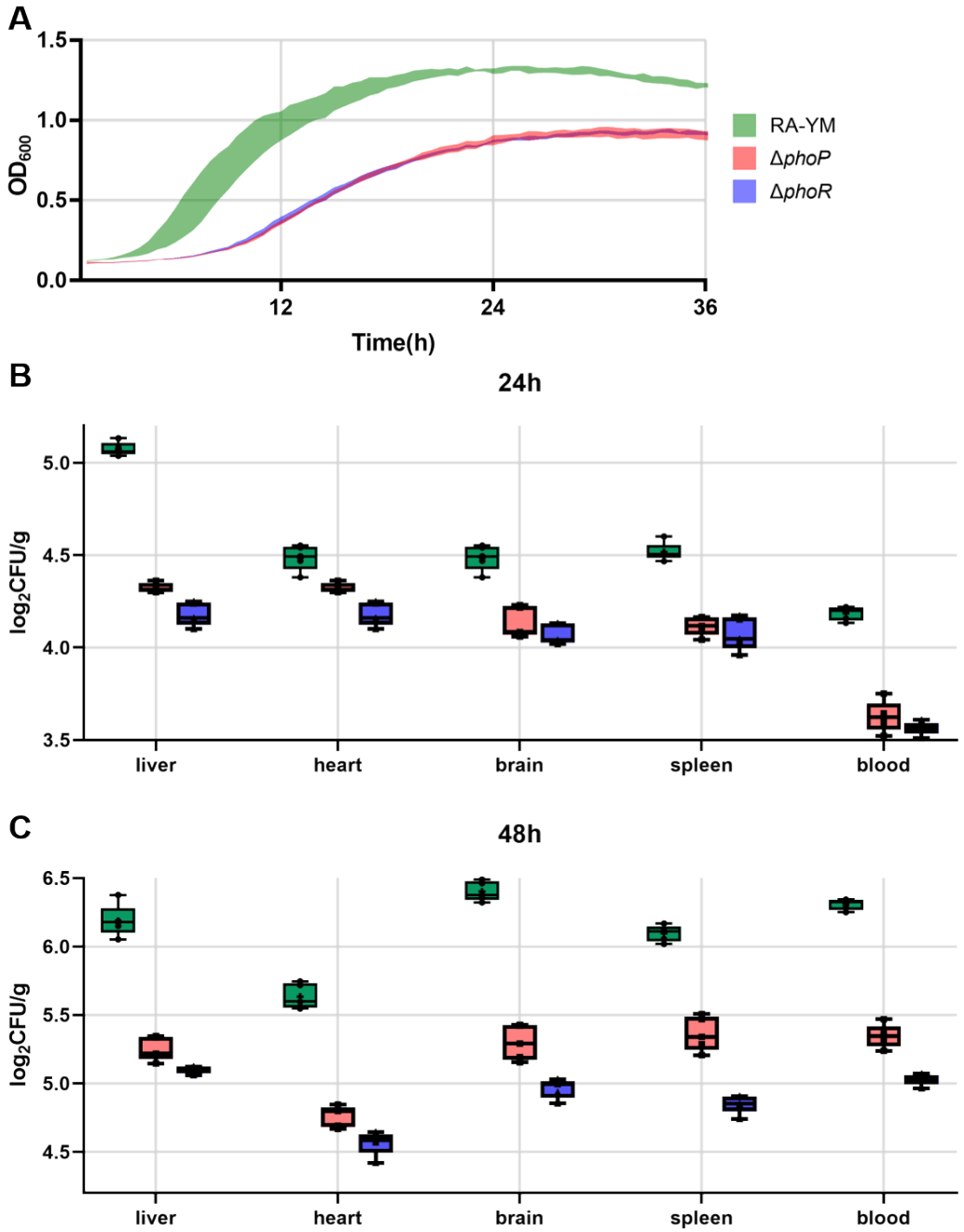

Figure 8. Biological characteristics of the RA-YM, Δ*phoP*, and Δ*phoR* strains. (A) The growth curves of Δ*phoP*, Δ*phoR,* and RA-YM strain in TSB. The indicated strains were grown to the exponential phase (OD_{600} = 0.6–0.8) in TSB, at which point they were harvested by centrifugation and resuspended to OD_{600} = 1 in TSB and then transferred to a new TSB medium in multiples of 1:100. OD_{600} was measured per 30 min, and five repetitions were

353 carried out for each strain. Standard deviation is depicted in colored shadow. (B and C)
354 Δ*phoP*, Δ*phoR,* and RA-YM loaded from ducks' blood and tissues infected after 24 h and 48
355 h respectively. 2 weeks old ducklings were challenged with 10^5 CFU of Δ*phoP*, Δ*phoR,* and
356 RA-YM. After 24 or 48 h, the blood and tissues were harvested and the CFU was determined
357 by the serial dilution and pour plate method.
358
359 At 24 h and 48 h after injection, the duckling liver, heart, spleen, and brain tissue infected
360 with PBS, RA-YM, Δ*phoP,* or Δ*phoR* strains fixed in formalin were subjected to
361 histopathologic examinations. The duckling tissues showed significant pathological changes
362 when infected with RA-YM at 24 h and 48 h. The abnormality was observed in the tissue
363 structures of the myocardial, liver, and spleen with necrosis and degeneration apparently
364 except in the brain, as shown by the black arrow at 24 h and 48 h (Fig 9). Some myocardial
365 fibers were arranged disorderly, and many inflammatory cells infiltrated the myocardial space
366 as shown by the red arrow (Fig 9). The hepatocytes were found to undergo extensive fatty
367 degeneration, as shown by the red arrow in live tissue (Fig 9). The structure of the spleen
368 tissue was abnormal, some lymphocytes were necrotic and degenerative, and the nucleus was
369 fragmented and pyknosis. The structure of brain tissue was abnormal, some neurons were
370 hyperchromatic and underwent pyknosis, and there was an evident phenomenon of
371 psychrophilic cells. The glial cells could be seen to undergo phagocytosis, as shown by the
372 green arrow in brain tissues (Fig 9). The tissues did not show obvious pathological changes
373 when infected with PBS, Δ*phoP,* and Δ*phoR*. The results showed that the pathological
374 changes in the tissues and organs of the ducklings were significantly reduced after 24 h and

375 48 h of infection with Δ*phoP* and Δ*phoR*. In conclusion, the pathogenicity of Δ*phoP* or

376 Δ*phoR* was significantly lower than that of the RA-YM. Thus, PhoP and PhoR were proven to

377 be virulence-related factors of *R. anatipestifer*.

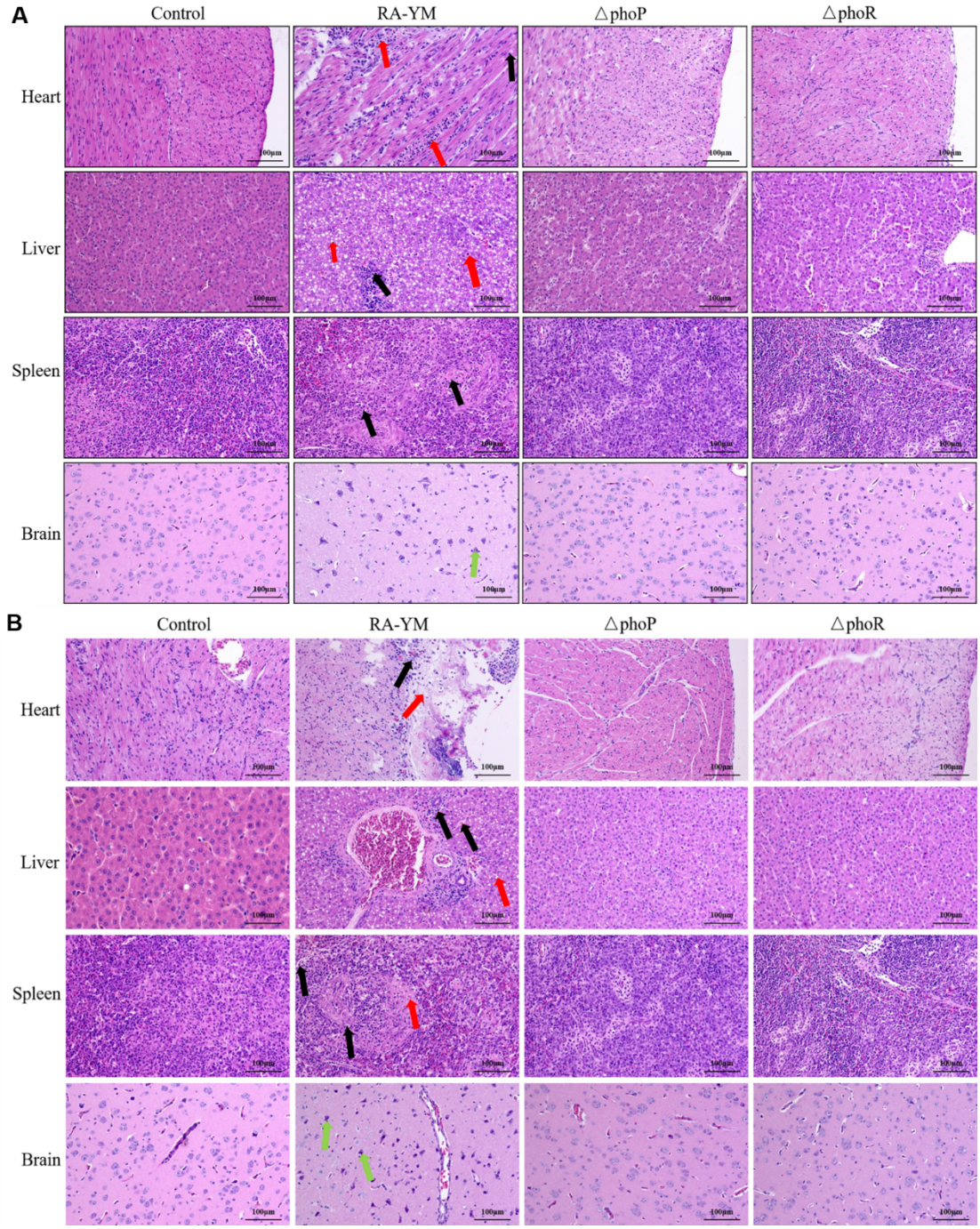

378

379 **Figure 9. Histopathological analysis of the duck tissues infected with RA-YM, Δ*phoP*,**

380 **and Δ*phoR*.** (A and B) The heart, liver, spleen, and brain samples were collected from the

381 infected ducks with RA-YM, Δ*phoP*, and Δ*phoR* at 24 h (A) and 48 h (B). The black arrow
382 represents the pathologic change of necrosis and degeneration in the tissues. The red arrow
383 represented the fatty degenerated hepatocytes in the hepatic tissues and disorder-arranged
384 myocardial fibers and the inflammatory cell which infiltrated the myocardial space in the
385 heart. The green arrow represents the phagocytosis surrounded by the glial cells in the brain.
386

387 Discussion

388 PhoP/PhoR is essential for pathogenicity in *R. anatipestifer*. Here, the regulatory mechanism
389 of PhoP was explored in *R. anatipestifer* by DAP-seq and RNA-seq. This study provided new
390 insight into how PhoP/PhoR regulates the transcriptome accordingly and established a new
391 model for studying transcriptional regulation. To identify the direct binding sites of PhoP, the
392 DAP-seq was analyzed to get a global view of the regulons. To study the directly regulated
393 genes, the RNA-seq was used to study the regulons of *phoP* after constructing the Δ*phoP* and
394 Δ*phoR* gene deletion strain. Finally, the direct regulons of PhoP were found and *phoP* and
395 *phoR* were identified as essential virulence-related factors for *R. anatipestifer*.
396 The PhoP/PhoR two-component system exists in most Gram-positive bacteria, and
397 PhoB/PhoR exists in most Gram-negative bacteria. The PhoP/PhoR and PhoB/PhoR TCS are
398 involved in regulating phosphate homeostasis. The expression of these TCS depends on the
399 concentration of phosphate in the environment and is upregulated to regulate the downstream-
400 related genes under low phosphate conditions, which are collectively called pho regulators
401 [42]. In addition to regulating phosphate homeostasis, PhoP/PhoR is also believed to regulate
402 other cellular processes such as biofilm formation, cell wall metabolism, vitamin metabolism,

and bacterial respiration [34]. Most importantly, PhoP/PhoR has also been shown to regulate the pathogenesis of many pathogens. The annotated homologs of PhoP and PhoR of *Bacillus anthracis* were significantly similar to the PhoP/PhoR proteins of other pathogens [16], PhoP/PhoR TCS has also been reported in *B. subtilis* [44], *Streptomyces Penicillium* [45], *M. tuberculosis* [46].

In many bacteria, such as *B. subtilis*, *Salmonella typhi*, and *M. tuberculosis, phoP* belongs to the member of pho regulator as the self-regulators [34]. The self-regulation of PhoP in the *R. anatipestifer* was first identified via EMSA, and the binding was located in region 156–121 upstream of the start codon ATG of *phoP*/*phoR* (Fig 3). PhoP is known to regulate the virulence-related genes in several pathogens, such as *Enterococcus faecalis*, *Corynebacterium pseudotuberculosis*, and *M. tuberculosis*, *E. coli* [47–50]. The PhoP/PhoR two-component system is very important for the virulence of *M. tuberculosis* and can be used as a potential target for developing anti-tuberculosis therapy [51]. Humans do not possess proteins of these two-component systems, so they are suitable targets for antibacterial drugs. Previous studies have shown that the biological characteristics of double genes deletion strain Δ*phoP*/*phoR* are the same as RA-YM and the Δ*phoP*/*phoR* double genes mutation strain virulence and the ability to damage the host tissues and organs were significantly lower, $LD_{50}>10^{10}$ CFU and hence could be considered to be an avirulent strain [21].

To further explore the function of *phoP*/*phoR* in *R. anatipestifer*, the DAP-seq was applied to investigate the PhoP-bind sites around the genome globally. To investigate the binding sites of PhoP on the genome of *R. anatipestifer*, the ChIP-seq, the commonly used method to study the global binding sites of transcription factors in the genome was initially used. The

425 experimental premise of ChIP-seq and accuracy of the enrichment of the binding-DNA were
426 found to have certain requirements for the purity and specificity of the antibody against RR.
427 A polyclonal antibody was prepared against PhoP and the antibody was purified by PhoP
428 affinity. The western blot results showed unexpected bands on the PVDF membrane when
429 testing the specificity of the antibody against the total protein of *R. anatipestifer*, which might
430 be due to the binding to the other transcription factors containing the winged helix-turn-helix
431 domain. Considering the confidence of the subsequent peak-calling for PhoP-binding regions,
432 the plan to perform ChIP-seq with antibody to PhoP was abandoned, and Δ*phoP* was not
433 constructed at that time. Another point considered was that we did not fully understand which
434 signals are sensed by the PhoP of *R. anatipestifer*, resulting in the inability to simulate the
435 regulation of DNA binding upon activating the response regulator. Finally, the DAP-seq was
436 applied to avoid and solve the mentioned problems. DAP-seq does not require a specific
437 antibody like the ChIP-seq, and only requires an affinity method for the tag-labeled response
438 regulator. Meanwhile, the transcription factors can be modified *in vitro* and then bind to
439 DNA, especially when the activation conditions of the response regulator are unknown.
440 From the peaks generated from DAP-seq data, 5 peaks (upstream regions of *phoPR*, *moxR*,
441 *KYF39_06865*, *dnaG,* and *dedA*) were identified via EMSA. The DNA binding domain of
442 PhoP was also investigated to find out whether it could bind the peaks independently, and the
443 EMSA results indicated the necessity of N-terminal RD (receiver domain) for the DNA-
444 binding ability of PhoP in *R. anatipestifer* (Fig 3B). For NarL in *E. coli*, the DBD was
445 inhibited by the N-terminal RD in the pattern that the C-terminal DBD folds back into the N-
446 terminal RD leading to the loss of the DNA-binding activity [52]. In this case,

447 phosphorylation is necessary for releasing the inhibition, allowing the RD dimerization or
448 oligomerization and DBD to bind to the target DNA. OmpR binds to DNA as a monomer
449 with high affinity resulting from the stimulated phosphorylation and subsequent dimerization
450 by RD, while OmpR-DBD binds to DNA with a low affinity incapable of transcriptional
451 initiation [53,54]. But in *B. subtilis* the opposite phenomenon was observed, the N-terminus
452 and C-terminus of PhoP were found to function independently and did not mutually inhibit
453 their domain functions [55]. We also wondered whether PhoP needs phosphorylation for
454 binding to the DNA or enhancing the DNA-binding ability. The EMSA results showed that
455 phosphorylation is not necessary for the DNA-binding *in vitro* and did not significantly
456 enhance the DNA-binding (Fig 4A and 4B). Similar situations were observed in the DNA
457 binding of ComE in *Streptococcus mutans* [35] and PhoP in *B. subtilis* [55]. Increasing
458 concentrations of acetyl-P or phosphoramidite were not significant for the DNA binding
459 ability of ComE, and there was a diminution of the extent of the shift-band that appeared in
460 EMSA instead probably due to the RR being already been phosphorylated endogenously
461 during the purification from *E. coli* BL21 (DE3). Spo0A is heterologously phosphorylated
462 and functional in DNA-binding when expressed in *E. coli*.[56]. Therefore, the Phos-tag SDS-
463 PAGE was utilized to investigate whether PhoP could be phosphorylated by acetyl-P *in vitro*,
464 and the results showed that PhoP could be phosphorylated *in vitro* with acetyl-P in a time-
465 dependent manner (Fig S2). Although the phosphorylated PhoP was observed as a shifted
466 band on the Phos-tag SDS-PAGE followed by CBB staining, the degree of shifting was not
467 like that evident after dimerization or oligomerization of proteins. To date, it remains
468 unknown whether phosphorylation is essential for the transcription regulation of PhoP, but

our analysis of PhoP-binding strongly supported that phosphorylation does not play a role in the DNA-binding ability *in vitro*. Future work will focus on whether phosphorylation would change the preference of the binding motif of PhoP, and whether the interaction between proteins exists *in vivo*.

Further, the single-gene deletion strains namely Δ*phoP* and Δ*phoP* respectively were successfully constructed. The growth curve showed that Δ*phoP* and Δ*phoP* have decreased growth rates at every time point compared to the WT, and the cell density of WT was higher than Δ*phoP* and Δ*phoP* in TSB. The RNA-seq was used for studying gene differential expression when *phoP* or *phoR* was deleted. The results of transcriptome analysis showed 136 genes to be differentially expressed between Δ*phoP* and RA-YM, including 45 down-regulated genes. There were 183 differentially expressed genes between Δ*phoR* and RA-YM, including 123 down-regulated genes. The DEGs generated from Δ*phoP* and Δ*phoR* were compared and 57 DEGs were differentially expressed in the same trend, including 35 DEGs downregulated and 22 DEGs upregulated when *phoR* or *phoP* was deleted. Combining the data of DAP-seq and RNA-seq revealed the PhoP-binding sites in the upstream regions of 50 DEGs in Δ*phoP*. When *phoP* was deleted, there were several candidate genes related to aerobic tolerance or anaerobic respiration metabolism among 50 DEGs: 2 cytochrome c, NosL, and an electron transfer flavoprotein subunit were upregulated while the Bat operon was downregulated. The Bat operon was first reported in *B. fragilis*, composed of *batA*, *batB*, *batC*, *batD,* and *batE*, and *B. fragilis* was found to lose its aerotolerance after *batD* was mutated by insertion [57]. In *Porphyromonas gingivalis*, researchers also believed that the Bat operon ensured the survival ability of the pathogenic bacteria in the early process of infection

491 at the aerobic sites, and the Bat complex was possibly involved in imparting resistance to
492 oxidative stress [58]. Dieppedale identified that the Bat operon was important for stress
493 resistance and intracellular survival of *Francisella tularensis* [59]. However, the aerotolerance
494 related to the Bat operon was studied in the anaerobic bacteria before, but there was no
495 relevant research on the facultative anaerobic bacteria or aerobic bacteria. The mRNA levels
496 of *batA* and *batC* were found to differ in different strains or different oxygen content
497 treatments. The genes *batA* and *batC* were upregulated when H_2O_2 was added and
498 downregulated either when treated anaerobic, or when *phoP* or *phoR* was deleted (Fig S3).
499 The Bat operon was speculated to play the role in resisting oxidative stress in *R. anatipestifer*,
500 and the Bat operon was directly regulated by PhoP (Fig S4). Notably, 23 of 57 DEGs were
501 candidate target genes of PhoP where 40% of up-regulated genes have PhoP-binding sites in
502 the upstream regions, and 12.5% of down-regulated genes have PhoP-binding sites,
503 suggesting that indirect regulation is the major mechanism of PhoP.
504 The effects of *phoP* and *phoR* genes on the pathogenicity of ducklings have been studied *in*
505 *vivo*. The results showed that the LD_{50} of Δ*phoP* and Δ*phoR* increased by 4.7×10^4 times and
506 1.0×10^5 times compared to the RA-YM respectively, and the number of bacterial tissues
507 loading of ducklings infected with Δ*phoP* and Δ*phoR* at 24 h and 48 h was found to be
508 significantly lower than RA-YM. The results of LD_{50} and pathogenicity to ducklings showed
509 that *phoP* and *phoR* were essential virulence-related factors of *R. anatipestifer*. The above
510 results showed that both *phoR* and *phoP* could affect the gene expression of *R. anatipestifer*,
511 and the correlation between the virulence and *phoR* was higher than that of *phoP*, which was
512 consistent with LD_{50}. The activation of the RR activity depends on its homologous HK and

513 has a direct interaction mechanism with RR. In previous studies, response regulators have a
514 major role in bacterial pathogenicity. Recently, more and more literature has reported
515 histidine kinase to also play a key role in bacterial pathogenicity. The MgtC virulence protein
516 of *S. Enteritidis* is necessary for its survival and virulence in mice [60], and the MgtC
517 virulence protein is conserved in several intracellular pathogens including *Mycobacterium*
518 [61]. Although MgtC protein plays a key role in the survival of macrophages, only a few
519 molecular targets have been identified. MgtC targets the phosphohistidine kinase and
520 activates phosphate transport. The mutation of PhoR single amino acid prevents the binding
521 to MgtC, which results in the loss of MgtC-mediated phosphate transport and the reduction of
522 bacterial replication in macrophages. This suggests that the MgtC-mediated phosphate
523 transport is necessary for *Salmonella*, but the *phoR* gene plays a major role [60]. The *phoP*
524 gene is an important virulence factor in *M. tuberculosis* but recently reported *phoR* gene also
525 plays the same role [62]. The phenotype of the *phoR* deletion strain of *M. tuberculosis* is
526 similar to that of the *phoP* mutant strain, indicating that PhoP and PhoR might affect the same
527 biochemical pathway, suggesting that PhoP and PhoR play an important role in regulating the
528 virulence of *M. tuberculosis*.
529 In conclusion, both *phoR* and *phoP* are closely related to the virulence of RA-YM, and the
530 virulence of *phoR* and *phoP* gene deletion strains in ducklings are significantly reduced. The
531 present study has reported the first application of the combination of DAP-seq with RNA-seq
532 to perform genome-wide identification of the two-component systems regulon in pathogenic
533 bacteria. The entire set of target genes was determined under the regulation of PhoP in *R.*
534 *anatipestifer* and it was evaluated as to how *phoP* and *phoR* contribute to pathogenicity. In

addition, this study has provided a more available and sufficient method for exploring the response regulatory proteins in other two-component systems. Future work will probe into the virulence contribution and aerotolerance by the PhoP-regulated genes for identifying the molecular basis for the acute virulence defect in Δ*phoP*, and the mechanism of *R. anatipestifer* resisting ROS. The *phoP* and *phoR* gene deletion strains can serve as candidate live vaccine strains of *R. anatipestifer* to be applicable as the ideal genetic engineering vector strains for the expression of foreign antigens.

Material and methods

Ethics statement

All the animal experiments were carried out in accordance with the recommendations in the Guide for the Care and Use of Laboratory Animals from Research Ethics Committee, Huazhong Agricultural University, Hubei, China. All procedures performed in studies involving animals were in accordance with the ethical standards of the institution or practice at which the studies were conducted.

Bacterial strains and growth conditions

All strains are listed in supplementary S1 Table. RA-YM and derivates were routinely grown in Tryptic Soy Broth (Becton, Dickinson and Company, Franklin Lake, New Jersey, USA) or on Tryptic Soy Agar plates (Becton, Dickinson and Company, Franklin Lake, New Jersey, USA) with 3% (v/v) supplemented newborn calf serum (NEWZERUM, Upper Riccarton, Christchurch, New Zealand) at 37˚C with 5% CO_2.

555 *E. coli* strain χ7213 is a strain autotrophic on diaminopimelic acid (DAP) which is used for
556 delivering plasmid into *R. anatipestifer* via transconjugation, and is grown in Lysogeny broth
557 (LB) or LB agar supplemented with 50 μg/mL of diaminopimelic acid (Sigma-Aldrich,
558 Darmstadt, Germany) [63]. *E. coli* DH5α λpir was used for the propagation of pRE112 [64] or
559 its derived plasmids. *E. coli* DH5α was used for routine cloning, and *E. coli* BL21 (DE3) was
560 used for overexpression of His_6-PhoP. Chloramphenicol, kanamycin and spectinomycin were
561 used at a final concentration of 50 μg/mL, 100 μg/mL and 100 μg/mL respectively.

562 ## Cloning, overexpression and purification of His_6-PhoP and His_6-
563 ## PhoP-DBD

564 The recombinant plasmids pET-28a-PhoP and pET-28a-PhoP-DBD, which were used for
565 producing the His_6-PhoP and pET-28a-PhoP-DBD respectively, were constructed as follows.
566 Taking His_6-PhoP as example, *phoP* gene was amplified by PCR using *Riemerella*
567 *anatipestifer* RA-YM genomic DNA as a template with primers PhoP-F and PhoP-R (S2
568 Table). The DNA fragment was then digested with *BamH* I and *EcoR* I and cloned into the
569 same restriction enzyme-digested pET-28a vector. The plasmid identified by Sanger
570 sequencing was transformed into *E. coli* BL21 (DE3) strain. *E. coli* BL21 (DE3) containing
571 pET-28a-PhoP was grown at 37 ℃ in LB supplemented with kanamycin until an OD_{600} of
572 0.4–0.6 was reached then 1 mM isopropyl-1-thio-b-D-galactopyranoside (IPTG) was added.
573 After 8 hours at 28 ℃, cells were harvested and then resuspended in bacteria lysis buffer (50
574 mM Tris-HCl, 100 mM NaCl, 1% Triton-X-100, 10% glycerin, pH 8.0). After being crushed
575 by a pressure cell disruptor three times followed by 15-min centrifugation at 10,000 g to keep
576 the supernatant, the unbroken cells and insoluble fraction were removed. Then His_6-PhoP was

577 isolated from cell lysates by passage over a Ni-NTA Starose 6 Fast Flow column (Nanotion
578 biotech., Suzhou, China) pre-equilibrated with Binding Buffer (50 mM Tris-HCl, 100 mM
579 NaCl, 10% glycerin, 5 mM imidazole, pH 8.0), washing with the same buffer followed by the
580 buffer with 50 mM imidazole, and then gradient eluting with 50-500 mM imidazole with a
581 gradient of 50 mM. The elution fraction containing His_6-PhoP was dialyzed in Binding Buffer
582 to remove the high concentration of imidazole and concentrated using an ultrafilter (Merck
583 KGaA, Darmstadt, Germany). SDS-PAGE and Western blot with an anti-His tag antibody
584 was used to confirm the purified protein (ABclonal, Wuhan, China).

585 **DNA-affinity-purification library preparation followed by high-**
586 **throughput sequencing**

587 Genomic DNA of *Riemerella anatipestifer* RA-YM was extracted using a Bacterial DNA Kit
588 (Omega Bio-tek, USA). Then, 10 μg of genomic DNA was sheared to length of 300–500 bp
589 using ultrasonication for 15 cycles with 3 s on and 7 s off on ice. The size of the sheared DNA
590 fragment was checked via 2% agarose gel, and then 2 μg of sheared genomic DNA was
591 mixed with purified His_6-PhoP in 200 μl Buffer A (10 mM Tris-HCl pH 7.5, 1 mM DTT, 50
592 mM KCl, 5 mM $MgCl_2$, 25% glycerol, and 50 mM acetyl phosphate) and incubated reactions
593 for 30 min at room temperature. 10 μl of this reaction was transferred to a 1.5 mL tube with
594 70 μL Buffer C (10mM Tris-HCl, pH 7.5, 5mM $MgCl_2$, 50mM KCl, 25% glycerol and
595 500mM imidazole) and labeled as the INPUT DNA. The 190 μL mixture was added 60 μL of
596 Ni-NTA agarose resin for 30 min that had been washed twice by Buffer B (10mM Tris-HCl,
597 pH 7.5, 5mM $MgCl_2$, 50mM KCl and 25% glycerol) via centrifuge at 100 x g for 2 min.
598 Centrifuged at 100 x g for 2 min, the mixture was washed with Buffer A three times to

599 remove the supernatant (unbound DNA), and incubated with 70 μL of Buffer C at room
600 temperature for 5 min to eluted His_6-PhoP. After centrifugation at 100 x g for 2 min, the
601 supernatant was labeled as the PhoP-bind DNA. The Rapid Plus DNA Lib Prep Kit for
602 Illumina (ABclonal, Wuhan, China) was used to prepare the PhoP-bind DNA and INPUT
603 DNA libraries for Illumina sequencing according to the manufacturer, with the PCR Index
604 Primers in Dual DNA Adapter 96 Kit for Illumina (ABclonal, Wuhan, China). Each
605 sequencing was performed on an Illumina NovaSeq 6000 platform up to 6 Gb data with
606 paired-end 150 nt reads (PE150) at Annoroad Gene Technology. DAP-seq original data were
607 uploaded to the NCBI Short Read Archive (SRA) with accession numbers (PRJNA818095).

608 ## RNA extraction and cDNA preparation

609 The RA-YM, Δ*phoP* or Δ*phoR* strain was cultured on TSA medium respectively, each strain
610 single colony was cultured in TSB medium at 37℃ overnight and then transferred to TSB
611 medium in multiples of 1:100. After shaking at 37℃ and 200 rpm, the bacteria were harvested
612 by centrifugation when OD_{600} reached 0.8. RNA was extracted from the harvested sample,
613 using Bacterial RNA Kit. cDNA was obtained by reverse transcription PCR of RNA using
614 HiScript II Reverse Transcriptase (Vazyme, Nanjing, China).

615 ## RNA-seq

616 The RA-YM, Δ*phoP* or Δ*phoR* strains were cultured on TSA medium respectively, each
617 strain single colony was cultured in TSB medium at 37℃ overnight, and then transferred to
618 TSB medium in multiples of 1:100. After shaking at 37℃ and 200 rpm, the collected bacterial
619 RNA was extracted when OD_{600} reached 0.8. RNA samples were sent to Wuhan Bena

Technology Co., Ltd. for transcriptome sequencing and analysis. RNA-Seq original data were uploaded to the NCBI Short Read Archive (SRA) with study accession numbers SRR14321696 - SRR14321704. (http://www.ncbi.nlm.nih.gov/sra).

Real-time qPCR

Total RNA from RA-YM and derivates were extracted and reverse transcribed into cDNA as previous described. qPCR was performed in technical duplicates with 5 µL ChamQ Universal SYBR qPCR Master Mix (Vazyme, Nanjing, China), 0.25 µL of each primer (10 µM; listed in S2 Table), 4.5 µL diluted cDNA sample in a 96-well PCR plate (Thermo Scientific, Massachusetts, USA). The plate was run in a Bio-Rad CFX96 machine (Bio-Rad, Hercules, California, USA). recA was chose as the reference gene. Results were analyzed with the comparative critical threshold cycle method.

Analysis of DAP-seq data and RNA-seq data

The quality of the raw pair-end reads from DAP-seq and RNA-seq were evaluated using FASTQC (www.bioinformatics. babraham.ac.uk/projects/fastqc/), and then low-quality reads and contamination were filtered using Trimmomatic [65]. The clean reads were aligned to the *Riemerella anatipestifer* RA-YM genome using Bowtie2 with default parameters. Unmapped reads and non-uniquely mapped reads (mapping quality < 30) were removed and PCR duplicate reads were removed with SAMtools [66]. To comprehensively analyze the multi-omics data from DAP-seq and RNA-seq, deepTools2 [67] was utilized to count the coverage through whole-genome with a bin size of 1 Mb, and the samples were normalized by reads

per kilobase per million mapped reads. Statistical analysis and data records Student's t-tests were used to compare gene expression data. For RNA-seq, the normalization of counts and detection of DEGs were performed by DESeq2 (the absolute value of fold change ≥ 2 and $P < 0.05$) [68] on R platform. For DAP-seq, MACS2 [69] was used to call the peaks from data with the following parameters -f BEDPE -g 2100000 -B -q 0.01. DeepTools was used to generate a bigWig file based on the comparison of two normalized BAM files, and visualized the continuous data in TBtools [33].

EMSA

The predicted motif located on the upstream region of candidate genes was synthesis as a biotin-labelled probe via annealing after 95 ℃ for 2min of a pair of reverse complementary primers one of them was 5' modified by biotin. All primers including biotin-modified primers were synthesized by Tsingke (Tsingke, Beijing, China) and listed in S2 Table. The Chemiluminescent EMSA Kit (Beyotime Biotechnology, Shanghai, China) was used according to the manufacturer's instructions. 100 ng biotin-labeled probe was mixed with 1-4 μg His_6-PhoP at 25 ℃ for 15 min. Pre-cooled 0.5× TBE was prepared that is the main buffer for electrophoresis and transformation and pre-electrophoresed the non-denatured PAGE gel. The mixture was then electrophoresed on a non-denatured PAGE gel (pre-electrophoresed for an hour at 100 V) in an ice-bath at 100 V for 120 min in 0.5× TBE, and the gel was transferred to an N+ nylon membrane (GE Amersham, United States) at 380 mA for 30min in 0.5× TBE. The UV crosslinking of the N+ nylon membrane was carried out for 30 min under an ultraviolet lamp (10 cm). The crosslinked N+ nylon membrane was incubated in Blocking

Buffer (Beyotime Biotechnology, China) on a horizontal shaker slowly for 30 min and then the Blocking Buffer was removed then add Blocking Buffer containing Streptavidin-HRP Conjugate (Beyotime Biotechnology, China) diluted at 1:2000 for 30 min on a horizontal shaker. Next, the N+ nylon membrane was washed for 10 min four times with Washing Buffer (Beyotime Biotechnology, China), and then transferred to Detection Equilibrium Solution (Beyotime Biotechnology, China) shaking for 10 min. At last, the bands were detected by BeyoECL Plus after dyeing (Beyotime Biotechnology, China).

Growth experiments

The growth curves of Δ*phoP*, Δ*phoR* and RA-YM strain in TSB. Indicated strains were grown to exponential phase (OD_{600} = 0.6-0.8) in TSB, at which point they were harvested by centrifugation and resuspended to OD_{600} = 1 in TSB and then transferred to TSB medium at the ratio of 1:100. 200μL diluted bacteria in TSB was transferred in a 200-well Honeycomb (Bioscreen). The plate was incubated at 37˚C in Bioscreen C MBR (Bioscreen, Finland) for 48 h and OD_{600} was measured every 30 min for the duration of growth.

Construction of *phoP* and *phoR* gene mutation strains

RA-YM genome as template, the left and right arm fragments of *phoP* and *phoR* genes were amplified by PCR. According to the sequence of spectinomycin resistance gene (Spec) in pIC 333 plasmid, primers were designed for overlap PCR to amplify resistance gene. The Spec, left and right arm fragments were linked by overlap extension PCR. pRE112 as suicide plasmid, Kpn Ⅰ and Sac I restriction sites were applied to construct recombinant suicide plasmids. *E. coli* χ7213 competent cells were transformed with pRE-PhoP-LSR or pRE-

682 PhoR-LSR, which served as the donor strain for transconjugation. Cells of donor strain and
683 RA-YM were washed and resuspended in 10 mM $MgSO_4$ three times, then mixed with a ratio
684 of 4:1 (1×10^9: 2.5×10^8) and dripped onto a sterile filter membrane disc (Φ 0.45 μm) which
685 was placed on TSA agar plate supplemented with 50 μg/ml of DAP before, followed by
686 incubation at 37°C for 12 hours. The bacterial cells were washed off from the disc and
687 resuspended with 10 mM $MgSO_4$ three times, and the cells plated onto TSA agar containing
688 spectinomycin followed by 48 h growth at 37°C with 5% CO_2. The colonies were picked and
689 target strains were identified by PCR with the primers list in S2 Table.

690 **Pathogenicity analysis of Δ*phoP* and Δ*phoR* strains in Ducklings**

691 The Δ*phoP*, Δ*phoR* strains and RA-YM strains were prepared in TSB medium and
692 centrifuged at 5000 rpm for 3 min, respectively. The strains were resuspended with PBS and
693 centrifuged again for 3 times. The OD_{600} value of the bacteria were determined. The bacterial
694 solution was diluted to 5.0×10^9, 5.0×10^8, 5.0×10^7, 5.0×10^6 and 5.0×10^5 CFU / mL,
695 respectively. 12-day old Cherry Valley ducks were divided into 16 groups, 10 in each group.
696 The specific grouping is shown in Table 2. Each flipper was injected with 0.2 mL bacterial
697 solution, and the control group was injected with the same amount of PBS. The apparent
698 changes of ducklings after bacterial injection were observed. The death situation was
699 recorded, and LD_{50} was calculated. 12-day old Cherry Valley ducks were divided into three
700 groups. The Δ*phoP*, Δ*phoR* strains and RA-YM strains were prepared same as above. Each
701 duck was inoculated with 0.2 mL (1.0×10^5 CFU) bacterial solution, and the control group
702 was injected with the same amount of sterilized PBS. After 24 hours and 48 hours of
703 inoculation, 5 ducklings were randomly selected for calculating bacterial load in tissues and

704 blood. Refer to published literature for detail operation methods. The ducklings infected with
705 the Δ*phoP*, Δ*phoR* strains and RA-YM strains were dissected to observe the pathological
706 changes, especially brain, heart, liver, spleen. The tissues were fixed in 10% formalin for
707 pathological section.

708

709 Acknowledgments

710 We are grateful for all members of the Li laboratory for helpful discussion and support.
711 Thanks Dr. Ke Xiao (Huazhong Agricultural University) for technical and equipment
712 assistance on DNA-library construction and multi-omics research. We thank Dr. Jianming
713 Zeng (University of Macau) for generously sharing their experience and codes.

714

715 Author Contributions

716 **Conceptualization:** Yang Zhang, Ying Wang

717 **Data curation:** Yang Zhang, Ying Wang

718 **Formal analysis:** Yang Zhang, Ying Wang, Zili Li

719 **Funding acquisition:** Zili Li

720 **Investigation:** Yang Zhang, Ying Wang, Yanhao Zhang, Yanhao Zhang, Chenxi Li

721 **Methodology:** Yang Zhang, Ying Wang, Zutao Zhou, Sishun Hu, Zili Li

722 **Project administration:** Yang Zhang, Ying Wang,Sishun Hu, Zili Li

723 **Resources:** Yang Zhang, Ying Wang, Zutao Zhou, Zili Li

724 **Software:** Yang Zhang

725 **Supervision:** Yang Zhang, Zili Li

Validation: Yang Zhang, Ying Wang

Visualization: Yang Zhang, Ying Wang

Writing – original draft: Yang Zhang, Ying Wang

Writing – review & editing: Yang Zhang, Zili Li

Reference

1. Hess C, Enichlmayr H, Jandreski-Cvetkovic D, Liebhart D, Bilic I, Hess M. Riemerella anatipestifer outbreaks in commercial goose flocks and identification of isolates by MALDI-TOF mass spectrometry. Avian Pathol J WVPA. 2013;42: 151–156. doi:10.1080/03079457.2013.775401

2. Segers P, Mannheim W, Vancanneyt M, De Brandt K, Hinz KH, Kersters K, et al. Riemerella anatipestifer gen. nov., comb. nov., the causative agent of septicemia anserum exsudativa, and its phylogenetic affiliation within the Flavobacterium-Cytophaga rRNA homology group. Int J Syst Bacteriol. 1993;43: 768–776. doi:10.1099/00207713-43-4-768

3. Pathanasophon P, Phuektes P, Tanticharoenyos T, Narongsak W, Sawada T. A potential new serotype of Riemerella anatipestifer isolated from ducks in Thailand. Avian Pathol J WVPA. 2002;31: 267–270. doi:10.1080/03079450220136576

4. Wang X, Ding C, Wang S, Han X, Hou W, Yue J, et al. The AS87_04050 gene is involved in bacterial lipopolysaccharide biosynthesis and pathogenicity of Riemerella anatipestifer. PloS One. 2014;9: e109962. doi:10.1371/journal.pone.0109962

5. Dou Y, Wang X, Yu G, Wang S, Tian M, Qi J, et al. Disruption of the M949_RS01915 gene changed the bacterial lipopolysaccharide pattern, pathogenicity and gene expression of Riemerella anatipestifer. Vet Res. 2017;48: 6. doi:10.1186/s13567-017-0409-6

6. Dou Y, Yu G, Wang X, Wang S, Li T, Tian M, et al. The Riemerella anatipestifer M949_RS01035 gene is involved in bacterial lipopolysaccharide biosynthesis. Vet Res. 2018;49: 93. doi:10.1186/s13567-018-0589-8

7. Tian X, Huang L, Wang M, Biville F, Zhu D, Jia R, et al. The functional identification of Dps in oxidative stress resistance and virulence of Riemerella anatipestifer CH-1 using a new unmarked gene deletion strategy. Vet Microbiol. 2020;247: 108730. doi:10.1016/j.vetmic.2020.108730

8. Guo Y, Hu D, Guo J, Wang T, Xiao Y, Wang X, et al. Riemerella anatipestifer Type IX

Secretion System Is Required for Virulence and Gelatinase Secretion. Front Microbiol. 2017;8: 2553. doi:10.3389/fmicb.2017.02553

9. Yuan H, Huang L, Wang M, Jia R, Chen S, Liu M, et al. Role of the gldK gene in the virulence of Riemerella anatipestifer. Poult Sci. 2019;98: 2414–2421. doi:10.3382/ps/pez028

10. Malhi KK, Wang X, Chen Z, Ding C, Yu S. Riemerella anatipestifer gene AS87_08785 encodes a functional component, GldK, of the type IX secretion system. Vet Microbiol. 2019;231: 93–99. doi:10.1016/j.vetmic.2019.03.006

11. Chen Z, Wang X, Ren X, Han W, Malhi KK, Ding C, et al. Riemerella anatipestifer GldM is required for bacterial gliding motility, protein secretion, and virulence. Vet Res. 2019;50: 43. doi:10.1186/s13567-019-0660-0

12. Stock AM, Robinson VL, Goudreau PN. Two-component signal transduction. Annu Rev Biochem. 2000;69: 183–215. doi:10.1146/annurev.biochem.69.1.183

13. Bourret RB, Hess JF, Borkovich KA, Pakula AA, Simon MI. Protein phosphorylation in chemotaxis and two-component regulatory systems of bacteria. J Biol Chem. 1989;264: 7085–7088.

14. Gonzalo-Asensio J, Malaga W, Pawlik A, Astarie-Dequeker C, Passemar C, Moreau F, et al. Evolutionary history of tuberculosis shaped by conserved mutations in the PhoPR virulence regulator. Proc Natl Acad Sci U S A. 2014;111: 11491–11496. doi:10.1073/pnas.1406693111

15. Salzberg LI, Botella E, Hokamp K, Antelmann H, Maaß S, Becher D, et al. Genome-wide analysis of phosphorylated PhoP binding to chromosomal DNA reveals several novel features of the PhoPR-mediated phosphate limitation response in Bacillus subtilis. J Bacteriol. 2015;197: 1492–1506. doi:10.1128/JB.02570-14

16. Aggarwal S, Somani VK, Gupta V, Kaur J, Singh D, Grover A, et al. Functional characterization of PhoPR two component system and its implication in regulating phosphate homeostasis in Bacillus anthracis. Biochim Biophys Acta Gen Subj. 2017;1861: 2956–2970. doi:10.1016/j.bbagen.2016.09.022

17. Tran T-K, Han Q-Q, Shi Y, Guo L. A comparative proteomic analysis of Salmonella typhimurium under the regulation of the RstA/RstB and PhoP/PhoQ systems. Biochim Biophys Acta. 2016;1864: 1686–1695. doi:10.1016/j.bbapap.2016.09.003

18. O'Loughlin JL, Spinner JL, Minnich SA, Kobayashi SD. Yersinia pestis two-component gene regulatory systems promote survival in human neutrophils. Infect Immun. 2010;78: 773–782. doi:10.1128/IAI.00718-09

19. Tobe T. The roles of two-component systems in virulence of pathogenic Escherichia coli

and Shigella spp. Adv Exp Med Biol. 2008;631: 189–199. doi:10.1007/978-0-387-78885-2_13

20. Wang Q, Chen M, Zhang W. A two-component signal transduction system contributes to the virulence of *Riemerella anatipestifer*. J Vet Sci. 2018;19: 260. doi:10.4142/jvs.2018.19.2.260

21. Wang Y, Lu T, Yin X, Zhou Z, Li S, Liu M, et al. A Novel RAYM_RS09735/RAYM_RS09740 Two-Component Signaling System Regulates Gene Expression and Virulence in Riemerella anatipestifer. Front Microbiol. 2017;8: 688. doi:10.3389/fmicb.2017.00688

22. Xie Y, Shao X, Zhang Y, Liu J, Wang T, Zhang W, et al. Pseudomonas savastanoi Two-Component System RhpRS Switches between Virulence and Metabolism by Tuning Phosphorylation State and Sensing Nutritional Conditions. mBio. 2019;10: e02838-18. doi:10.1128/mBio.02838-18

23. Fu J, Qin R, Zong G, Liu C, Kang N, Zhong C, et al. The CagRS Two-Component System Regulates Clavulanic Acid Metabolism via Multiple Pathways in Streptomyces clavuligerus F613-1. Front Microbiol. 2019;10: 244. doi:10.3389/fmicb.2019.00244

24. de Castro PA, Chen C, de Almeida RSC, Freitas FZ, Bertolini MC, Morais ER, et al. ChIP-seq reveals a role for CrzA in the Aspergillus fumigatus high-osmolarity glycerol response (HOG) signalling pathway. Mol Microbiol. 2014;94: 655–674. doi:10.1111/mmi.12785

25. Park DM, Akhtar MS, Ansari AZ, Landick R, Kiley PJ. The bacterial response regulator ArcA uses a diverse binding site architecture to regulate carbon oxidation globally. PLoS Genet. 2013;9: e1003839. doi:10.1371/journal.pgen.1003839

26. Rajeev L, Luning EG, Mukhopadhyay A. DNA-affinity-purified chip (DAP-chip) method to determine gene targets for bacterial two component regulatory systems. J Vis Exp JoVE. 2014. doi:10.3791/51715

27. Rajeev L, Luning EG, Dehal PS, Price MN, Arkin AP, Mukhopadhyay A. Systematic mapping of two component response regulators to gene targets in a model sulfate reducing bacterium. Genome Biol. 2011;12: R99. doi:10.1186/gb-2011-12-10-r99

28. Rolfe MD, Ter Beek A, Graham AI, Trotter EW, Asif HMS, Sanguinetti G, et al. Transcript profiling and inference of Escherichia coli K-12 ArcA activity across the range of physiologically relevant oxygen concentrations. J Biol Chem. 2011;286: 10147–10154. doi:10.1074/jbc.M110.211144

29. Liu X, De Wulf P. Probing the ArcA-P modulon of Escherichia coli by whole genome transcriptional analysis and sequence recognition profiling. J Biol Chem. 2004;279: 12588–12597. doi:10.1074/jbc.M313454200

30. Salmon KA, Hung S, Steffen NR, Krupp R, Baldi P, Hatfield GW, et al. Global gene expression profiling in Escherichia coli K12: effects of oxygen availability and ArcA. J Biol Chem. 2005;280: 15084–15096. doi:10.1074/jbc.M414030200

31. Paudel A, Panthee S, Hamamoto H, Grunert T, Sekimizu K. YjbH regulates virulence genes expression and oxidative stress resistance in Staphylococcus aureus. Virulence. 2021;12: 470–480. doi:10.1080/21505594.2021.1875683

32. Bessaiah H, Pokharel P, Habouria H, Houle S, Dozois CM. yqhG Contributes to Oxidative Stress Resistance and Virulence of Uropathogenic Escherichia coli and Identification of Other Genes Altering Expression of Type 1 Fimbriae. Front Cell Infect Microbiol. 2019;9: 312. doi:10.3389/fcimb.2019.00312

33. Chen C, Chen H, Zhang Y, Thomas HR, Frank MH, He Y, et al. TBtools: An Integrative Toolkit Developed for Interactive Analyses of Big Biological Data. Mol Plant. 2020;13: 1194–1202. doi:10.1016/j.molp.2020.06.009

34. Birkey SM, Liu W, Zhang X, Duggan MF, Hulett FM. Pho signal transduction network reveals direct transcriptional regulation of one two-component system by another two-component regulator: Bacillus subtilis PhoP directly regulates production of ResD. Mol Microbiol. 1998;30: 943–953. doi:10.1046/j.1365-2958.1998.01122.x

35. Hung DCI, Downey JS, Kreth J, Qi F, Shi W, Cvitkovitch DG, et al. Oligomerization of the response regulator ComE from Streptococcus mutans is affected by phosphorylation. J Bacteriol. 2012;194: 1127–1135. doi:10.1128/JB.06565-11

36. Kinoshita-Kikuta E, Kusamoto H, Ono S, Akayama K, Eguchi Y, Igarashi M, et al. Quantitative monitoring of His and Asp phosphorylation in a bacterial signaling system by using Phos-tag Magenta/Cyan fluorescent dyes. Electrophoresis. 2019;40: 3005–3013. doi:10.1002/elps.201900261

37. Chimalakonda G, Ruiz N, Chng S-S, Garner RA, Kahne D, Silhavy TJ. Lipoprotein LptE is required for the assembly of LptD by the beta-barrel assembly machine in the outer membrane of Escherichia coli. Proc Natl Acad Sci U S A. 2011;108: 2492–2497. doi:10.1073/pnas.1019089108

38. Vishnu US, Sankarasubramanian J, Gunasekaran P, Rajendhran J. Novel Vaccine Candidates against Brucella melitensis Identified through Reverse Vaccinology Approach. Omics J Integr Biol. 2015;19: 722–729. doi:10.1089/omi.2015.0105

39. Park HK, Myung SC, Kim W. Comparative transcriptomic analysis of streptococcus pseudopneumoniae with viridans group streptococci. BMC Microbiol. 2012;12: 77. doi:10.1186/1471-2180-12-77

40. Xia K, Han C, Xu J, Liang X. Transcriptome response of Acetobacter pasteurianus Ab3 to high acetic acid stress during vinegar production. Appl Microbiol Biotechnol.

2020;104: 10585–10599. doi:10.1007/s00253-020-10995-0

41. Sund CJ, Rocha ER, Tzianabos AO, Tzinabos AO, Wells WG, Gee JM, et al. The Bacteroides fragilis transcriptome response to oxygen and H2O2: the role of OxyR and its effect on survival and virulence. Mol Microbiol. 2008;67: 129–142. doi:10.1111/j.1365-2958.2007.06031.x

42. Wanner BL. Gene regulation by phosphate in enteric bacteria. J Cell Biochem. 1993;51: 47–54. doi:10.1002/jcb.240510110

43. Whole-Genome Sequence Analysis and Genome-Wide Virulence Gene Identification of Riemerella anatipestifer Strain Yb2 | Applied and Environmental Microbiology. [cited 4 Apr 2022]. Available: https://journals.asm.org/doi/10.1128/AEM.00828-15?url_ver=Z39.88-2003&rfr_id=ori:rid:crossref.org&rfr_dat=cr_pub%20%200pubmed

44. Guo Q, Li S, Lu X, Li B, Ma P. PhoR/PhoP two component regulatory system affects biocontrol capability of Bacillus subtilis NCD-2. Genet Mol Biol. 2010;33: 333–340. doi:10.1590/S1415-47572010005000032

45. Sola-Landa A, Moura RS, Martín JF. The two-component PhoR-PhoP system controls both primary metabolism and secondary metabolite biosynthesis in Streptomyces lividans. Proc Natl Acad Sci U S A. 2003;100: 6133–6138. doi:10.1073/pnas.0931429100

46. Baker JJ, Johnson BK, Abramovitch RB. Slow growth of Mycobacterium tuberculosis at acidic pH is regulated by phoPR and host-associated carbon sources. Mol Microbiol. 2014;94: 56–69. doi:10.1111/mmi.12688

47. Teng F, Wang L, Singh KV, Murray BE, Weinstock GM. Involvement of PhoP-PhoS homologs in Enterococcus faecalis virulence. Infect Immun. 2002;70: 1991–1996. doi:10.1128/IAI.70.4.1991-1996.2002

48. Tiwari S, da Costa MP, Almeida S, Hassan SS, Jamal SB, Oliveira A, et al. C. pseudotuberculosis Phop confers virulence and may be targeted by natural compounds. Integr Biol Quant Biosci Nano Macro. 2014;6: 1088–1099. doi:10.1039/c4ib00140k

49. Chesne-Seck M-L, Barilone N, Boudou F, Gonzalo Asensio J, Kolattukudy PE, Martín C, et al. A point mutation in the two-component regulator PhoP-PhoR accounts for the absence of polyketide-derived acyltrehaloses but not that of phthiocerol dimycocerosates in Mycobacterium tuberculosis H37Ra. J Bacteriol. 2008;190: 1329–1334. doi:10.1128/JB.01465-07

50. Alteri CJ, Lindner JR, Reiss DJ, Smith SN, Mobley HLT. The broadly conserved regulator PhoP links pathogen virulence and membrane potential in Escherichia coli. Mol Microbiol. 2011;82: 145–163. doi:10.1111/j.1365-2958.2011.07804.x

51. He X, Wang L, Wang S. Structural basis of DNA sequence recognition by the response regulator PhoP in Mycobacterium tuberculosis. Sci Rep. 2016;6: 24442. doi:10.1038/srep24442

52. Baikalov I, Schröder I, Kaczor-Grzeskowiak M, Grzeskowiak K, Gunsalus RP, Dickerson RE. Structure of the Escherichia coli response regulator NarL. Biochemistry. 1996;35: 11053–11061. doi:10.1021/bi960919o

53. Rhee JE, Sheng W, Morgan LK, Nolet R, Liao X, Kenney LJ. Amino acids important for DNA recognition by the response regulator OmpR. J Biol Chem. 2008;283: 8664–8677. doi:10.1074/jbc.M705550200

54. Yoshida T, Qin L, Egger LA, Inouye M. Transcription regulation of ompF and ompC by a single transcription factor, OmpR. J Biol Chem. 2006;281: 17114–17123. doi:10.1074/jbc.M602112200

55. Liu W, Hulett FM. Bacillus subtilis PhoP binds to the phoB tandem promoter exclusively within the phosphate starvation-inducible promoter. J Bacteriol. 1997;179: 6302–6310. doi:10.1128/jb.179.20.6302-6310.1997

56. Ladds JC, Muchová K, Blaskovic D, Lewis RJ, Brannigan JA, Wilkinson AJ, et al. The response regulator Spo0A from Bacillus subtilis is efficiently phosphorylated in Escherichia coli. FEMS Microbiol Lett. 2003;223: 153–157. doi:10.1016/S0378-1097(03)00321-5

57. Tang YP, Dallas MM, Malamy MH. Characterization of the BatI (Bacteroides aerotolerance) operon in Bacteroides fragilis: isolation of a B. fragilis mutant with reduced aerotolerance and impaired growth in in vivo model systems. Mol Microbiol. 1999;32: 139–149. doi:10.1046/j.1365-2958.1999.01337.x

58. Meuric V, Gracieux P, Tamanai-Shacoori Z, Perez-Chaparro J, Bonnaure-Mallet M. Expression patterns of genes induced by oxidative stress in Porphyromonas gingivalis. Oral Microbiol Immunol. 2008;23: 308–314. doi:10.1111/j.1399-302X.2007.00429.x

59. Dieppedale J, Sobral D, Dupuis M, Dubail I, Klimentova J, Stulik J, et al. Identification of a putative chaperone involved in stress resistance and virulence in Francisella tularensis. Infect Immun. 2011;79: 1428–1439. doi:10.1128/IAI.01012-10

60. Choi S, Choi E, Cho Y-J, Nam D, Lee J, Lee E-J. The Salmonella virulence protein MgtC promotes phosphate uptake inside macrophages. Nat Commun. 2019;10: 3326. doi:10.1038/s41467-019-11318-2

61. Le Moigne V, Belon C, Goulard C, Accard G, Bernut A, Pitard B, et al. MgtC as a Host-Induced Factor and Vaccine Candidate against Mycobacterium abscessus Infection. Infect Immun. 2016;84: 2895–2903. doi:10.1128/IAI.00359-16

62. Xing D, Ryndak MB, Wang L, Kolesnikova I, Smith I, Wang S. Asymmetric Structure of the Dimerization Domain of PhoR, a Sensor Kinase Important for the Virulence of Mycobacterium tuberculosis. ACS Omega. 2017;2: 3509–3517. doi:10.1021/acsomega.7b00612

63. Roland K, Curtiss R, Sizemore D. Construction and evaluation of a delta cya delta crp Salmonella typhimurium strain expressing avian pathogenic Escherichia coli O78 LPS as a vaccine to prevent airsacculitis in chickens. Avian Dis. 1999;43: 429–441.

64. Edwards RA, Keller LH, Schifferli DM. Improved allelic exchange vectors and their use to analyze 987P fimbria gene expression. Gene. 1998;207: 149–157. doi:10.1016/s0378-1119(97)00619-7

65. Bolger AM, Lohse M, Usadel B. Trimmomatic: a flexible trimmer for Illumina sequence data. Bioinforma Oxf Engl. 2014;30: 2114–2120. doi:10.1093/bioinformatics/btu170

66. Li H, Handsaker B, Wysoker A, Fennell T, Ruan J, Homer N, et al. The Sequence Alignment/Map format and SAMtools. Bioinforma Oxf Engl. 2009;25: 2078–2079. doi:10.1093/bioinformatics/btp352

67. Ramírez F, Ryan DP, Grüning B, Bhardwaj V, Kilpert F, Richter AS, et al. deepTools2: a next generation web server for deep-sequencing data analysis. Nucleic Acids Res. 2016;44: W160-165. doi:10.1093/nar/gkw257

68. Love MI, Huber W, Anders S. Moderated estimation of fold change and dispersion for RNA-seq data with DESeq2. Genome Biol. 2014;15: 550. doi:10.1186/s13059-014-0550-8

69. Zhang Y, Liu T, Meyer CA, Eeckhoute J, Johnson DS, Bernstein BE, et al. Model-based analysis of ChIP-Seq (MACS). Genome Biol. 2008;9: R137. doi:10.1186/gb-2008-9-9-r137

Supporting information captions

Figure S1. Expression of His_6-PhoP and His_6-PhoP-DBD. (A) Purification of His_6-PhoP by Ni-NTA affinity, and eluents with different concentrations of imidazole visualized using SDS-PAGE. His_6-PhoP is supposed to be 31.23 kD. (B) His_6-PhoP after ultrafiltration concentration using an ultrafilter (Merck KGaA, Germany). (C) Purification of His_6-PhoP-DBD by Ni-NTA affinity, and eluents with different concentrations of imidazole visualized

using SDS-PAGE.

Figure S2. Identification of phosphorylation of PhoP *in vitro*. The phosphorylation of PhoP *in vitro* via a different duration of incubation with acetyl-P was shown via Phos-tag SDS-PAGE followed by CBB staining.

Figure S3. mRNA levels of *batA* and *batC* in different strains or different oxygen content treatments. RA-YM and derivates were grown in TSB to exponential phase, and the bacterial were harvested and resuspended in new TSB with OD_{600} adjusted to 1.0. Subsequently, the following conditions were applied for RA-YM: aerobic (50 mM H_2O_2 was added to 1mL RA-YM), control (1mL RA-YM), anaerobic (culture 1mL RA-YM in anaerobic incubator). All adjusted bacteria were grown for 2h and harvested for RNA extraction. *recA* was chose as the reference gene.

Figure S4. Schematic organization of Bat operon. The upper line showed that PhoP directly binds to the upstream region of *moxR* to enhance transcription of Bat operon, and the PhoP-binding site showed in red with the binding sequence shown below. Bat operon of *F. Tularensis* LVS, *B. Fragilis* strain YCH46 and *P. gingivalis* strain W83 were shown for comparison. Distance between adjacent genes is shown above the sequence (negative number indicates the number of overlapping bases, positive number indicates the number of separated bases).

S1 Table. Strains and plasmids used in this study

S2 Table. Oligonucleotides used in this study

S3 Table. 59 DEGs both in Δ*phoP* and Δ*phoR* compared with WT

S4 Table. Death of ducklings inoculated the Δ*phoP,* Δ*phoR* and RA-YM strain

S5 Table. All peaks-calling analysis of DAP-seq data. Column B: the start position of peaks; Column C: the end position of peaks; Column E: absolute position of peaks.

S6 Table. Comparative analysis of RNA-seq data for Δ*phoP*/Δ*phoR* and WT, and selected peaks-calling analysis of DAP-seq data

The reference sequence of *R. anatipestifer* RA-YM (ACCESSION: NZ_CP079205) was used for mapping, feature counting and differential gene expression analysis. **Column A:** Locus tag of *R. anatipestifer* RA-YM; **Column B-G:** All output from DESeq2 for Δ*phoP* and WT, **Column D-E:** Statistical analysis of differential gene expression including standard error estimate for the log2-fold change estimate (lfcSE, column D) and adjusted p-value (column G); **Column H-M:** All output from DESeq2 for Δ*phoR* and WT, **Column J-M:** Statistical analysis of differential gene expression including standard error estimate for the log2-fold change estimate (lfcSE, column J) and adjusted p-value (column M); **Column N-V:** MACS2 output of the genes which abs_summit located in -500:100 region of the start codon ATG of gene, Column Q-T: Location information of the peaks.

Data Availability: RNA-seq raw data have be deposited in the SRA databases with study accession numbers SRR14321696-SRR14321704, and DAP-seq raw data have been deposited with SRR18392563-SRR18392566. RA-YM genome assembled by PacBio platform have been deposited in NCBI/GenBank under the accession CP079205.1.